JCB Journal of Cell Biology

ARTICLE

Nap1 and Kap114 co-chaperone H2A-H2B and facilitate targeted histone release in the nucleus

Ho Yee Joyce Fung[1,2], Jenny Jiou[1], Ashley B. Niesman[1,2], Natalia E. Bernardes[1], and Yuh Min Chook[1]

Core histones, synthesized and processed in the cytoplasm, must be chaperoned as they are transported into the nucleus for nucleosome assembly. The importin Kap114 transports H2A-H2B into the yeast nucleus, where Ran^{GTP} facilitates histone release. Kap114 and H2A-H2B also bind the histone chaperone Nap1, but how Nap1 and Kap114 cooperate in transport and nucleosome assembly remains unclear. Here, biochemical and structural analyses show that Kap114, H2A-H2B, and a Nap1 dimer ($Nap1_2$) associate in the absence and presence of Ran^{GTP} to form equimolar complexes. A previous study had shown that Ran^{GTP} reduces Kap114's ability to chaperone H2A-H2B, but a new cryo-EM structure of the $Nap1_2$•H2A-H2B•Kap114•Ran^{GTP} complex explains how both Kap114 and $Nap1_2$ interact with H2A-H2B, restoring its chaperoning within the assembly while effectively depositing it into nucleosomes. Together, our results suggest that Kap114 and $Nap1_2$ provide a sheltered path that facilitates the transfer of H2A-H2B from Kap114 to $Nap1_2$, ultimately directing its specific deposition into nucleosomes.

Introduction

Formation of new nucleosomes to pack newly replicated DNA during the S-phase of the cell cycle begins with the rapid synthesis of core histones H3, H4, H2A, and H2B, followed by their swift transport into the nucleus. Exposure of these very basic polypeptides to the cellular environment is deeply deleterious as they form toxic aggregates easily (Hogan and Foltz, 2021; Singh et al., 2010). Therefore, core histones are thought to be always chaperoned and never free (Elsässer and D'Arcy, 2013; Hammond et al., 2017). As H3 and H4 emerge from translating ribosomes, they are folded into H3-H4 heterodimers by heat shock proteins and folding chaperones, acetylated at several lysine side chains (Benson et al., 2006; Campos et al., 2010; Tagami et al., 2004), and then passed to histone chaperone ASF1 and *H. sapiens* (*Hs*) Importin-4 or its *S. cerevisiae* (*Sc*) homolog Kap123 for transport across the nuclear pore complex (NPC) into the nucleus (Baake et al., 2001; Bernardes and Chook, 2020; Mühlhäusser et al., 2001; Schwamborn et al., 1998).

Unfortunately, the steps of H2A-H2B biosynthesis and processing have not been delineated. However, selective ribosome profiling studies showed no association of *Sc* importins with the nascent chains of H2A and H2B (Seidel et al., 2023), suggesting that H2A-H2B processing may also involve interaction with heat shock proteins and histone chaperones prior to importin-binding for nuclear import. The heat shock proteins/folding chaperones for H2A and H2B have not been identified, and the only known H2A-H2B histone chaperone in the *Sc* cytoplasm is nucleosome assembly protein 1 or Nap1 (Chen et al., 2016; Huang et al., 2020; Mosammaparast et al., 2002). H2A-H2B also binds several *Hs* Nap1 homologs in human cells (Chang et al., 1997; Okuwaki et al., 2010). The importin primarily responsible for H2A-H2B nuclear import is also known. Multiple studies have reported on H2A and H2B import by the homologous and orthologous importins *Sc* Karyopherin-114 (Kap114) and *Hs* Importin-9 (IMP9/IPO9) (Baake et al., 2001; Jäkel et al., 2002; Jiou et al., 2023; Johnson-Saliba et al., 2000; Kimura et al., 2017; Mosammaparast et al., 2001, 2002; Mühlhäusser et al., 2001; O'Reilly et al., 2011; Padavannil et al., 2019).

H2A and H2B contain disordered N- and C-terminal tails and central alpha helices that fold together into the globular H2A-H2B histone-fold domain, with very basic surfaces that bind DNA in the nucleosome (Fig. 1 A) (Luger et al., 1997). These same surfaces are shielded when H2A-H2B binds the *Sc* Nap1 dimer ($Nap1_2$), which is mostly localized to the yeast cytoplasm where it chaperones newly synthesized and folded H2A-H2B (Aguilar-Gurrieri et al., 2016; Calvert et al., 2008; Mosammaparast et al., 2002; Park et al., 2008). Nap1 also has well-known roles in the nucleus, including nucleosome assembly/remodeling, transcription, DNA repair, and mitosis, suggesting that it may shuttle between the nucleus and the cytoplasm (Aguilar-Gurrieri et al., 2016; Altman and Kellogg, 1997; Andrews

[1]Department of Pharmacology, University of Texas Southwestern Medical Center, Dallas, TX, USA; [2]Department of Biophysics, University of Texas Southwestern Medical Center, Dallas, TX, USA.

Correspondence to Yuh Min Chook: yuhmin.chook@utsouthwestern.edu

J. Jiou's current address is The Walter and Eliza Hall Institute of Medical Research, Parkville, Australia.

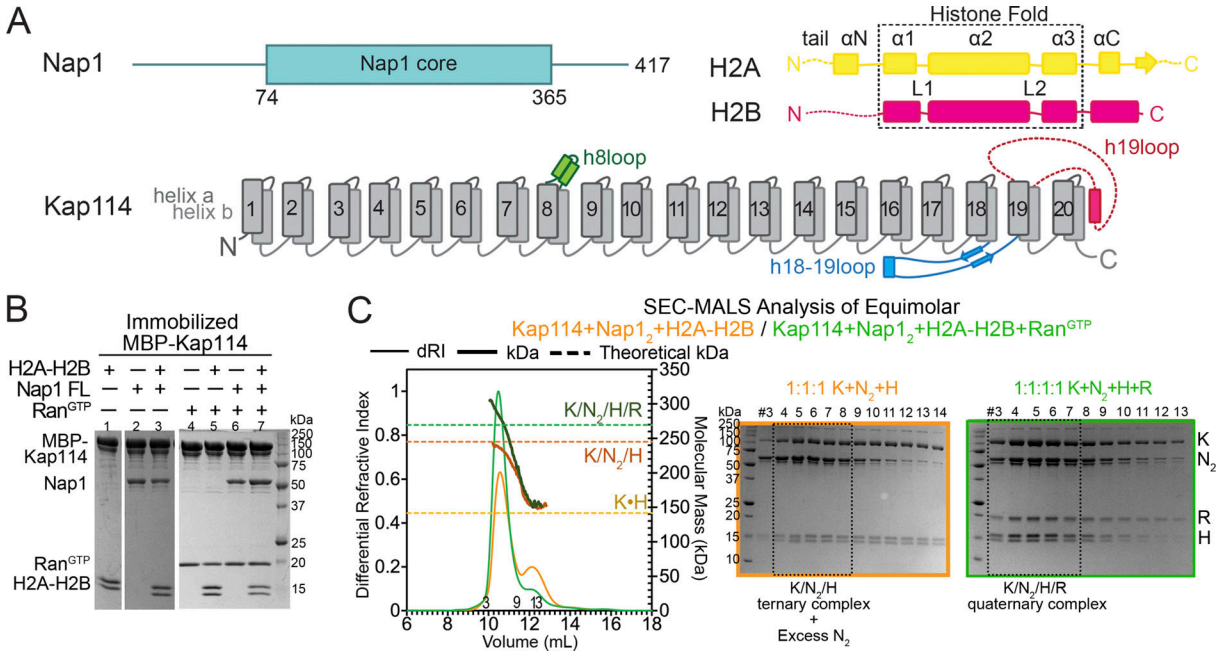

Figure 1. **Interactions between Kap114, Nap1, H2A-H2B, and Ran^{GTP}. (A)** Organization schematics of the Nap1 (cyan), H2A (yellow), H2B (magenta), and Kap114 (gray, long loops labeled) polypeptides. **(B)** Pull-down assay with immobilized MBP-Kap114 (1 µM) ± equimolar $Nap1_2$ ± Ran^{GTP}. **(C)** SEC-MALS analysis of equimolar Kap114, $Nap1_2$, and H2A-H2B mixtures without (orange) and with Ran^{GTP} (green). Left panel: differential refractive index (dRI, left y-axis, thin lines) and molecular mass (kDa, right y-axis, thick lines) traces, with theoretical masses of the Kap114•H2A-H2B (K•H), Kap114/$Nap1_2$/H2A-H2B (K/N_2/H), and Kap114/$Nap1_2$/H2A-H2B/Ran^{GTP} (K/N_2/H/R) complexes marked with dashed lines. Right panels: Coomassie-stained SDS-PAGE of peak fractions. When Ran^{GTP} is absent, the presence of a minor peak that matches K•H suggests the likely presence of some free Nap1 oligomers. Controls in Figs. S1 and S2. Source data are available for this figure: SourceData F1.

et al., 2010; Chen et al., 2016; Del Rosario and Pemberton, 2008; Dronamraju et al., 2017; Hsu et al., 2019; Kellogg and Murray, 1995; Krajewski, 2020; Levchenko and Jackson, 2004; Mazurkiewicz et al., 2006; Moshkin et al., 2013; Nagae et al., 2023; Park et al., 2005; Sharma and Nyborg, 2008; Vlijm et al., 2012). Genetic interaction of *Sc* Nap1 with Kap114 and with Ran binding proteins Yrb1 and Yrb2 have been reported, and the histone chaperone was also reported to be a cofactor for H2A-H2B nuclear import by Kap114 (Mosammaparast et al., 2002; Straube et al., 2010; Zlatanova et al., 2007). Furthermore, immunoprecipitation (IP) showed Kap114 association with both Nap1 and H2A-H2B in the yeast cytosolic extract and the Ran^{GTP}-rich nuclear extract, suggesting that the three proteins are associated in both the cytoplasm and the nucleus (Mosammaparast et al., 2002, 2005).

The mode of H2A-H2B recognition by Kap114/IMP9 is well understood: the superhelical Kap114 wraps around the H2A-H2B histone-fold domain, occluding the histone's DNA-binding surfaces and functioning as a histone chaperone (Jiou et al., 2023; Liao et al., 2020). Unlike most importin•cargo complexes, which are dissociated by the GTPase Ran^{GTP}, Kap114•H2A-H2B forms a stable ternary complex with Ran^{GTP}. This complex alters the interactions between Kap114 and H2A-H2B, facilitating histone release (Jiou et al., 2023). Although the interaction between Kap114 and H2A-H2B, both in the absence and presence of Ran^{GTP}, is well characterized, the role of Nap1 as a co-import factor and its influence on nucleosome assembly remains unknown.

Here, we used biochemical analyses and cryo-EM structure determination to reveal the quaternary $Nap1_2$•H2A-H2B•Kap114•Ran^{GTP} complex and its cytosolic counterpart. In this assembly, Ran^{GTP} binds to the N-terminal HEAT repeats of Kap114 while the H2A-H2B domain is sequestered by Nap1 and the C-terminal HEAT repeats of Kap114. DNA competition and nucleosome assembly assays confirmed that in the presence of Ran^{GTP}, Kap114 and Nap1 cooperate to shield H2A-H2B from non-specific aggregation with DNA and transfer H2A-H2B effectively and specifically into nucleosomes.

Results

Interactions between Kap114, Nap1, H2A-H2B, and Ran^{GTP}

Previous reports of biochemical and structural studies of Kap114•H2A-H2B and $Nap1_2$•H2A-H2B complexes, as well as pull-down studies of Kap114 and Nap1 from yeast lysates have informed on binary interactions between these proteins (Aguilar-Gurrieri et al., 2016; Jiou et al., 2023; Mosammaparast et al., 2002, 2005). Here, we confirm these findings using analytical ultracentrifugation (AUC) and size exclusion chromatography multiangle light scattering (SEC-MALS) analyses with purified recombinant Kap114, Nap1, and H2A-H2B proteins. Nap1 alone is a mixture of dimers and tetramers (Fig. S1 A), while Nap1 binds H2A-H2B to form a mixture of a Nap1 dimer ($Nap1_2$) bound to one H2A-H2B ($Nap1_2$•H2A-H2B) and larger Nap1/H2A-H2B assemblies (Fig. S1 B). Nap1 binds Kap114 to form a 1:1 Kap114:$Nap1_2$ complex (Fig. S1, A and C).

Next, we focused on interactions between the Kap114, Nap1, and H2A-H2B, in the absence and presence of Ran^{GTP}. Immobilized MBP-Kap114 pulled down Nap1 in the absence and presence of H2A-H2B; Kap114 also pulled down H2A-H2B in the absence and presence of Nap1 (Fig. 1 B and Fig. S1, D–F). SEC-MALS analysis showed the Kap114, $Nap1_2$, and H2A-H2B together forming a complex that matches the theoretical mass of a 1:1:1 Kap114/$Nap1_2$/H2A-H2B complex (Fig. 1 C and Fig. S1 G).

All importins bind Ran^{GTP} tightly, usually causing importin • cargo dissociation to release cargo in the nucleus (Dasso, 2002; Görlich et al., 1996; Hahn and Schlenstedt, 2011). However, a few exceptions have been reported, such as the very tight-binding TBP, which is released from Kap114 only at its target gene promoters (Liao et al., 2023; Pemberton et al., 1999). The Kap114/IMP9-H2A-H2B interaction is another exception as Ran^{GTP} binds Kap114/IMP9 • H2A-H2B to form a stable ternary Ran^{GTP} • Kap114/IMP9 • H2A-H2B complex (Fig. 4 A) (Jiou et al., 2023; Shaffer et al., 2023). Similarly, Kap114-Nap1 interaction persists in the presence of Ran^{GTP} as shown by pull-down assays and AUC analysis (Fig. 1 B and Fig. S2, A–C). SEC-MALS analysis showed that an equimolar mix of Kap114, $Nap1_2$, H2A-H2B, and Ran^{GTP} produced a major peak consistent with a complex that contains one molecule of each of the four proteins (Fig. 1 C).

Structure determination of the Kap114/$Nap1_2$/H2A-H2B/Ran^{GTP} complex

We assembled the quaternary Kap114/$Nap1_2$/H2A-H2B/Ran^{GTP} complex and solved the cryo-EM structure to 2.9 Å resolution (Table 1; Fig. 2 A; and Fig. S2, E–H) (Fung et al., 2024a, 2024b, 2024c). For comparison, we also performed cryo-EM analysis with a mixture of Kap114, $Nap1_2$, and excess H2A-H2B without Ran^{GTP}, which produced a heterogenous mixture of particles that included unliganded $Nap1_2$, the binary Kap114 • H2A-H2B complex, and small populations of two different assemblies containing Kap114, $Nap1_2$, and H2A-H2B (Fig. 2 B; Table S1; and Fig. S3). Excess histone in the sample had destabilized the Kap114/$Nap1_2$/H2A-H2B ternary complex (more discussion in Fig. S1). Structures of the two ternary Kap114/$Nap1_2$/H2A-H2B complexes are shown in Fig. 2 B and Fig. S3, for comparison with the quaternary Kap114/$Nap1_2$/H2A-H2B/Ran^{GTP} complex (additional discussion in Fig. S3 legend) (Jiou et al., 2024a, 2024b, 2024c).

The final cryo-EM map of the Kap114/$Nap1_2$/H2A-H2B/Ran^{GTP} complex is well-defined for Kap114 and Ran^{GTP} but the local resolution and map feature for $Nap1_2$ and H2A-H2B are poor. Local refinement produced a 4.0 Å map with improved map features. We built the structure of the quaternary complex using initial models from two other structures: (1) Ran^{GTP} bound to the N-terminal HEAT repeats of Kap114 from the Ran^{GTP} • Kap114 • H2A-H2B structure (PDB: 8F1E, Fig. 2 C) (Jiou et al., 2023) and (2) Kap114 repeats h17-h20 bound to $Nap1_2$ and H2A-H2B from the $Nap1_2$ • H2A-H2B • Kap114 structure obtained in this study (Fig. 2 B). We named the quaternary assembly the $Nap1_2$ • H2A-H2B • Kap114 • Ran^{GTP} complex (Fig. 2 A).

$Nap1_2$ • H2A-H2B • Kap114 • Ran^{GTP} resembles one of the ternary complexes, the $Nap1_2$ • H2A-H2B • Kap114 complex, except that no Ran^{GTP} is bound in the latter (Fig. 2, A and B). In both complexes, H2A-H2B is sandwiched between the C-terminal HEAT repeats of Kap114 and one subunit of the $Nap1_2$ (Fig. 2, A and B). In the quaternary $Nap1_2$ • H2A-H2B • Kap114 • Ran^{GTP} complex, Ran^{GTP} binds to HEAT repeats h1–4, 8, and 12–14 of Kap114 in the same way as in the Ran^{GTP} • Kap114 • H2A-H2B structure (Fig. 2, A and C). Comparison of the ternary and quaternary complexes shows that Ran-binding stabilizes a Kap114 conformation with an N-terminus closer to the bound H2A-H2B, but not as close as in the Ran^{GTP} • Kap114 • H2A-H2B structure where $Nap1_2$ is absent (Fig. S4 A).

The $Nap1_2$ β-hairpin and Kap114 h19loop are binding hotspots

In both the quaternary $Nap1_2$ • H2A-H2B • Kap114 • Ran^{GTP} and ternary $Nap1_2$ • H2A-H2B • Kap114 complexes, H2A-H2B interacts with the C-terminal HEAT repeats of Kap114 just like in other H2A-H2B-bound Kap114 structures, covering an extensive surface area of ~1,600 $Å^2$ (Fig. S4 B). The smaller (~120 $Å^2$) Kap114-$Nap1_2$ interface in $Nap1_2$ • H2A-H2B • Kap114 • Ran^{GTP} (and in $Nap1_2$ • H2A-H2B • Kap114) involves the β-hairpin of one $Nap1_2$ subunit (residues E288, R290 and Q292) contacting the Kap114 h19loop and the h20b helix (Fig. 2 D, left). The $Nap1_2$–histone interface involves acidic residues of the α4–6 helices of one $Nap1_2$ subunit contacting basic residues of the H2A αN and α1 helix (Fig. 2 D, right).

We mutated Nap1 residues that participate in Kap114-$Nap1_2$ and $Nap1_2$–histone interactions to assess their importance in forming quaternary and ternary complexes (Fig. 3 A, controls in Fig. S4 C). Alanine mutations of the $Nap1_2$ β-hairpin residues E288, R290, and Q292 (mutant β_{ERQ}) that contact Kap114 abolished $Nap1_2$ pull-down by MBP-Kap114 in the absence and presence of H2A-H2B and Ran^{GTP}. However, mutations of $Nap1_2$ residues E194, D201, and D205 (mutant $\alpha5/6_{mut}$) that contact H2A-H2B did not affect ternary or quaternary complex formation. These results support the importance of the $Nap1_2$ β-hairpin for Kap114-binding, in contrast to $Nap1_2$-H2A-H2B interactions, which are less important for ternary and quaternary complex formation.

We also mutated contact residues in Kap114 (Fig. 3 B). The Kap114 h19loop binds the $Nap1_2$ β-hairpin and it is therefore not surprising that truncating the loop (Kap114 Δh19L) abolished Kap114-Nap1 pull-down and formation of the ternary and quaternary complexes. However, mutating just D928 and D929 or Y939 and D942 (mutant Kap114 DD_{AA} and YD_{AA}) that contact $Nap1_2$ in the $Nap1_2$ • H2A-H2B • Kap114 • Ran^{GTP} and $Nap1_2$ • H2A-H2B • Kap114 structures did not affect Kap114-Nap1 pull-down. There are nearby acidic/electronegative Kap114 side chains that may also interact with the $Nap1_2$ β-hairpin (Fig. 2 D).

In summary, mutagenesis results indicate that although the interfaces between the $Nap1_2$ β-hairpin and Kap114 h19loop in both the ternary and quaternary structures are relatively small, these interactions are essential for binding (Fig. 3 C). Therefore, these results validate the cryo-EM structures of both $Nap1_2$ • H2A-H2B • Kap114 • Ran^{GTP} and $Nap1_2$ • H2A-H2B • Kap114 complexes. Our structural and biochemical results are also consistent with previously published results that suggested the importance of the Nap1 β-hairpin for nuclear localization of Nap1 in the yeast nuclei (Hodges et al., 2005; Mosammaparast et al., 2002, 2005).

Table 1. **Cryo-EM data collection, refinement, and validation statistics**

	$Nap1_2$·H2A-H2B·Kap114·Ran^{GTP}			$Nap1_2$·H2A-H2B·Kap114		
	Consensus map EMD-44151	**Locally refined map for $Nap1_2$·H2A-H2B EMD-44150**	**Composite map PDB: 9B3I EMD-44141**	**Consensus map EMD-44140**	**Locally refined map for $Nap1_2$·H2A-H2B EMD-44137**	**Composite map PDB: 9B3F EMD-44136**
Data collection and processing						
Magnification (X)	165,000			105,000		
Voltage (kV)	300			300		
Electron exposure ($e^-/Å^2$)	50			52		
Defocus range (μm)	0.9–2.2			1.5–2.5		
Pixel size (Å)	0.738			0.83		
Symmetry imposed	C1			C1		
Initial particle images (no.)	1,381,753			4,314,112		
Final particle images (no.)	133,516			113,011		
Map resolution (Å)	2.88	3.97		3.54	5.62	
FSC threshold	0.143					
Refinement						
Initial model used (PDB code)			8F1E, 9B3F			AF-P53067-F1, 8F1E, 9B23
Model composition						
Non-hydrogen atoms			14,951			13,451
Protein residues			1,854			1,668
Mean *B* factors ($Å^2$)						
Protein/Ligand			112.36/40.96			317.38
R.m.s. deviations						
Bond lengths (Å)			0.006			0.002
Bond angles (°)			0.781			0.505
CCvolume/mask			0.74/0.73			0.70/0.70
Validation						
MolProbity score			1.55			1.46
Clashscore			10.80			7.64
Poor rotamers (%)			0.24			0
Ramachandran plot						
Favored (%)			98.20			97.82
Allowed (%)			1.80			2.18
Disallowed (%)			0			0
CaBLAM outliers (%)			0.82			1.04
EMRinger score			2.45			0.94

Kap114 and $Nap1_2$: Co-chaperoning H2A-H2B in the absence of Ran^{GTP}

Nap1 and Kap114/*Hs* IMP9 had previously been identified as highly effective histone chaperones that prevent aggregation of H2A-H2B with DNA (Chang et al., 1997; Chen et al., 2016; Huang et al., 2020; Jiou et al., 2023; Mosammaparast et al., 2002; Padavannil et al., 2019). Consistent with their histone chaperone function, the $Nap1_2$ and Kap114 proteins in $Nap1_2$•H2A-H2B•Kap114 shield substantial portions (~1,800 $Å^2$) of the nucleosomal H3-H4 and DNA binding regions of H2A-H2B (Fig. 4 A). We performed DNA competition assays to probe the H2A-H2B chaperoning activity of Kap114 and $Nap1_2$, individually and together, within an equimolar ternary complex.

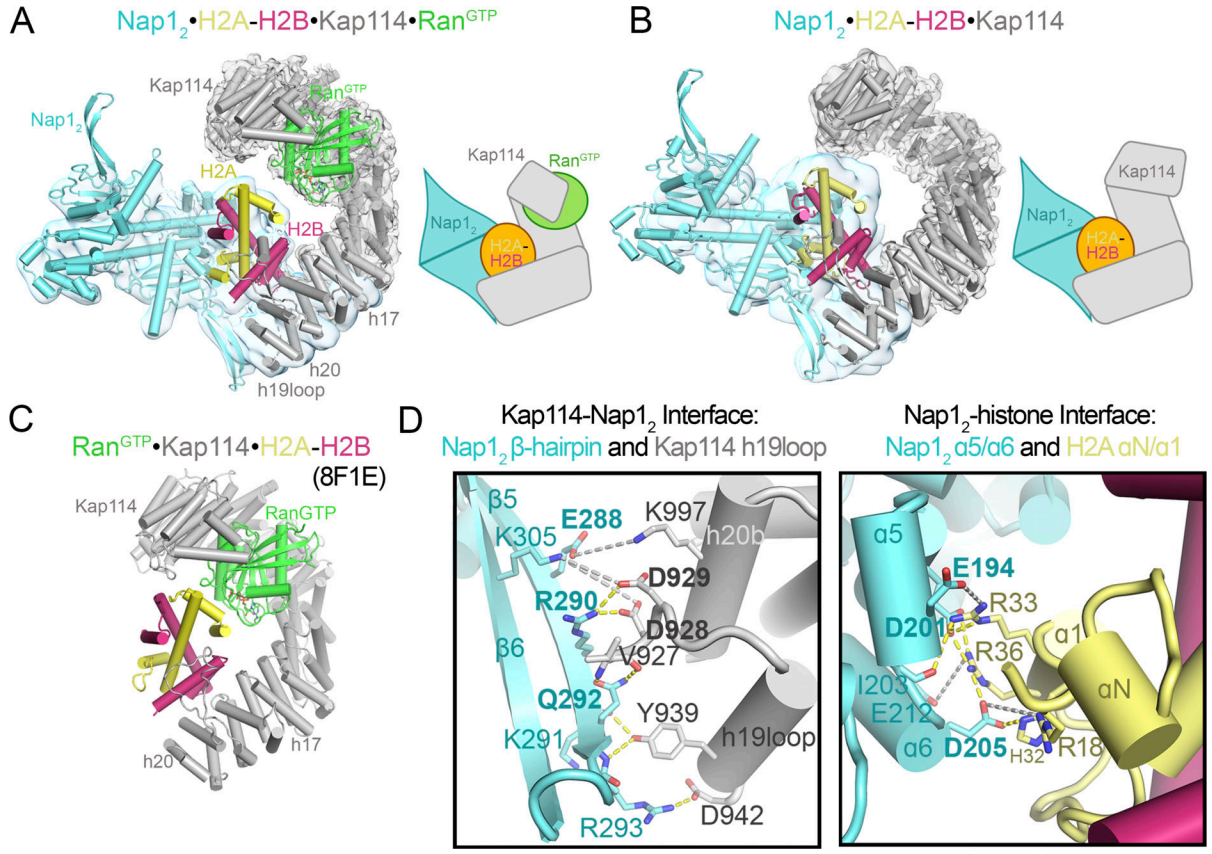

Figure 2. **Structure of the Nap1$_2$•H2A-H2B•Kap114•Ran^{GTP} complex. (A)** The Nap1$_2$•H2A-H2B•Kap114•Ran^{GTP} structure, with the consensus/local refined maps (gray/cyan) overlayed and a cartoon schematic on the right. **(B)** The Nap1$_2$•H2A-H2B•Kap114 structure shown is as in A. **(C)** The Ran^{GTP}•Kap114•H2A-H2B structure (8F1E). **(D)** Kap114-Nap1$_2$ contacts (left) and H2A-H2B-Nap1$_2$ contacts (right) in the Nap1$_2$•H2A-H2B•Kap114 structure. Dashed lines show intermolecular contacts <4.0 Å (yellow) and <8.0 Å (light gray). See more in Figs. S2, S3, and S4.

In this assay, H2A-H2B chaperoning would result in the disappearance of low-mobility DNA•H2A-H2B bands and the appearance of high-mobility–free DNA bands. We performed the experiments by either assembling DNA•H2A-H2B first and then titrating in Nap1$_2$ and/or Kap114 (Fig. 4 B) or assembling complexes of H2A-H2B with Kap114 and/or Nap1$_2$ first before titrating them into DNA (Fig. 4 C). To ensure a stable and intact ternary complex, we added Kap114 and/or Nap1$_2$ to DNA•H2A-H2B in an equimolar ratio, such as in lanes 5, 8, and 11 in EtBr gels (left) of Fig. 4, B and C, to avoid excess histone, which we know destabilizes the ternary complex (Fig. S1). Regardless of the order of addition, Kap114 and Nap1$_2$ together chaperone H2A-H2B from aggregation with DNA more effectively than either Kap114 or Nap1$_2$ alone.

Both Nap1 and Kap114 individually chaperoned H2A-H2B, decreasing low-mobility DNA•H2A-H2B bands and producing free DNA bands (Fig. 4 B). Interestingly, Nap1$_2$ is a more effective chaperone than Kap114 (Fig. 4 B, left gel: lanes 3–5 versus 6–8) even though the Nap1$_2$•H2A-H2B interface (~800 Å^2) is smaller than the Kap114•H2A-H2B interface (~2,200 Å^2). It is possible that dynamic interactions of the Nap1$_2$ C-terminal tail (not present in the Nap1$_2$•H2A-H2B structure) and Nap1$_2$ oligomerization with H2A-H2B may provide additional shielding of H2A-H2B (Aguilar-Gurrieri et al., 2016; Ohtomo et al., 2023).

Most importantly, the presence of both Kap114 and Nap1$_2$ enhances the chaperoning of H2A-H2B compared to when either is present alone (Fig. 4 B, left gel: compare lanes 5, 8, versus 11). This enhanced chaperoning occurs despite less histone surface being shielded in the Nap1$_2$•H2A-H2B•Kap114 complex (~1,600 Å^2) compared to the binary Kap114•H2A-H2B structure (~2,200 Å^2). We propose that additional surfaces of the histone, when bound to both Kap114 and Nap1$_2$, become inaccessible beyond the interfaces depicted in Fig. 4 A due to steric hindrance. For instance, although Nap1$_2$ in Nap1$_2$•H2A-H2B•Kap114 does not form <4 Å contacts with the DNA-binding region at the H2B α1 helix, it is <10 Å away, close enough to likely restrict access of other macromolecules to the histone (Fig. 4 A). Furthermore, the ternary complex is dynamic and the Nap1$_2$•H2A-H2B•Kap114 structure represents only one configuration of an ensemble of possible conformations (Fig. S3 B).

In summary, the structural and biochemical results above support Kap114 and Nap1$_2$ in the Nap1$_2$•H2A-H2B•Kap114 ternary complex cooperating to effectively co-chaperone H2A-H2B.

Kap114/Nap1 co-chaperoning and nucleosome assembly in the presence of Ran^{GTP}

The nuclear/quaternary Nap1$_2$•H2A-H2B•Kap114•Ran^{GTP} complex buries ~1,900 Å^2 of the H2A-H2B surface. Within this

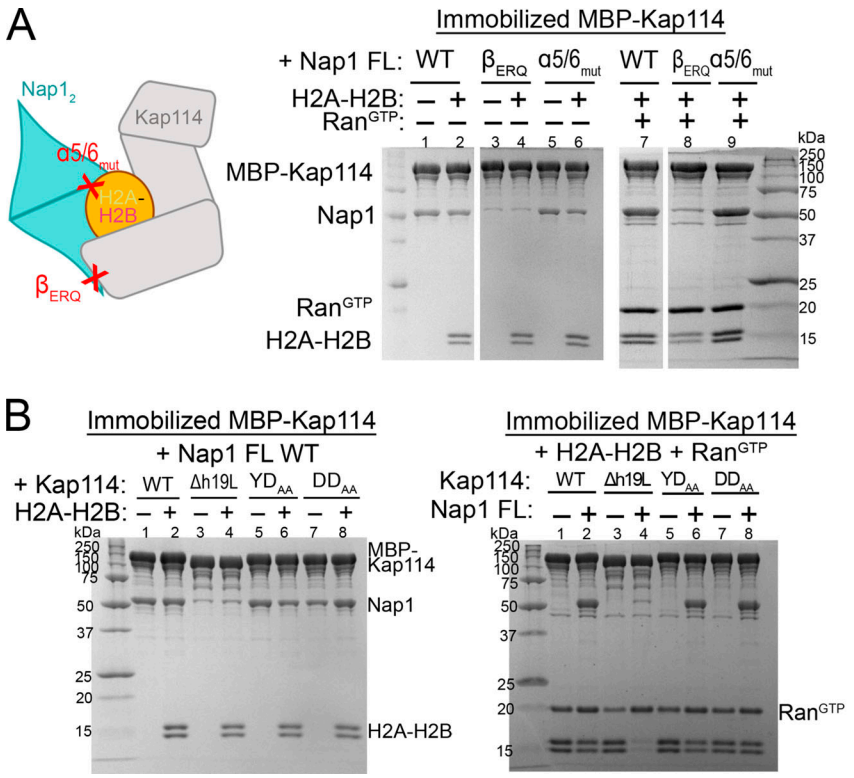

C

Pull-down assays

Proteins in assay	Bound to iK H	N_2	R
iK + H	+		
iK + N_2		+	
iK + R			+
iK + H + R	+		+
iK + N_2 + R		+	+
iK + $N_2\beta_{ERQ}$		–	
iK + H + $N_2\beta_{ERQ}$	+	–	
iK + H + $N_2\beta_{ERQ}$ + R	–	–	+
iK + $N_2\alpha5/6_{mut}$		+	
iK + H + $N_2\alpha5/6_{mut}$	+	+	
iK + H + $N_2\alpha5/6_{mut}$ + R	+	+	+
iK Δh19L + N_2		–	
iK Δh19L + H + N_2	+	–	
iK Δh19L + H + R	+		+
iK Δh19L + H + N_2 + R	–	–	+
iK YD_{AA}/DD_{AA} + N_2		+	
iK YD_{AA}/DD_{AA} + H + N_2	+	+	
iK YD_{AA}/DD_{AA} + H + R	+		+
iK YD_{AA}/DD_{AA} + H + N_2 + R	+	+	+

Figure 3. **The $Nap1_2$ β-hairpin and Kap114 h19loop are binding hotspots. (A)** Pull-down assay with equimolar MBP-Kap114 (1 µM), $Nap1_2$ (WT, β-hairpin mutant β_{ERQ} (E288A/R290A/Q292A) or histone-binding site mutant $\alpha5/6_{mut}$ (E194A/D201A/D205A), as indicated by schematic on the left) ± H2A-H2B ± Ran^{GTP}. Bounds proteins were visualized by Coomassie-stained SDS-PAGE. Controls in Fig. S4 C. **(B)** Kap114 h19loop mutants Δh19L (h19loop deleted), YD_{AA} (Y939A/D942A), and DD_{AA} (D928A/D929A) in pull-down assay as in A. **(C)** Summary of pull-down assays with immobilized MBP-Kap114 (iK). Source data are available for this figure: SourceData F3.

complex, $Nap1_2$ and Kap114 collectively shield the DNA binding interfaces of H2A-H2B, mirroring the arrangement observed in the cytosolic/ternary $Nap1_2$ • H2A-H2B • Kap114 structure (Fig. 5 A). The similarity in protein arrangements between the ternary and quaternary complexes suggests that, even in the presence of Ran^{GTP}, Kap114 and $Nap1_2$ likely continue to prevent H2A-H2B from aggregating with DNA. To test this hypothesis, we conducted DNA competition assays using Kap114, H2A-H2B, with and without $Nap1_2$ and titrated in Ran^{GTP} (Fig. 5, B and C).

In the absence of Ran^{GTP}, Kap114 alone can chaperone H2A-H2B. However, its efficacy as a histone chaperone decreases substantially in the presence of the GTPase (Fig. 5 B, compare lane 1 with lanes 2–5). Interestingly, when both $Nap1_2$ and Kap114 are present, H2A-H2B chaperoning remains unaffected by the presence of Ran^{GTP} (Fig. 5, compare lane 6 with lanes 7–10). This indicates that the histone is chaperoned effectively by Kap114 and $Nap1_2$ within the quaternary/nuclear $Nap1_2$ • H2A-H2B • Kap114 • Ran^{GTP} complex.

We also performed nucleosome assembly assays to assess the impact of Kap114, $Nap1_2$, and Ran^{GTP} on H2A-H2B deposition into tetrasomes, leading to nucleosome formation (Fig. 6, A and B). The results corroborate previous findings that $Nap1_2$ allows H2A-H2B deposition into nucleosomes (Fig. 6 A, lanes 5–7) (Andrews et al., 2010). In contrast, Kap114 inhibits H2A-H2B deposition into nucleosomes (Fig. 6 A, lanes 8–10) (Jiou et al., 2023). When both $Nap1_2$ and Kap114 are present, as in the ternary $Nap1_2$ • H2A-H2B • Kap114 complex, H2A-H2B can still be deposited into nucleosomes, like with $Nap1_2$ alone (Fig. 6 A, compare lanes 11–13 with 5–7). In the presence of both Ran^{GTP} and Kap114, as in the Ran^{GTP} • Kap114 • H2A-H2B complex, the GTPase facilitates histone release from Kap114, thus promoting nucleosome formation (Fig. 6 A, lanes 14–16). However, Ran^{GTP} • Kap114 • H2A-H2B does not effectively shield H2A-H2B from aggregation with DNA, consistent with the low mobility DNA • H2A-H2B bands and smear marked with white asterisks in lane 16 of Fig. 6 A. When $Nap1_2$, Kap114 and Ran^{GTP} are all present, as in the quaternary $Nap1_2$ • H2A-H2B • Kap114 • Ran^{GTP} complex, H2A-H2B deposition is more effective than either $Nap1_2$ alone or the ternary $Nap1_2$ • H2A-H2B • Kap114 complex (compare lanes 6, 12 and 18 of Fig. 6 A).

In summary, Kap114 and $Nap1_2$ in the quaternary $Nap1_2$ • H2A-H2B • Kap114 • Ran^{GTP} complex cooperate to chaperone H2A-H2B. Without $Nap1_2$, Ran^{GTP} would bind Kap114 • H2A-H2B, reorienting the bound histone and increasing its exposure to DNA and non-specific interactions. However, $Nap1_2$ binding H2A-H2B alongside Kap114 in the nuclear/quaternary $Nap1_2$ • H2A-H2B • Kap114 • Ran^{GTP} complex shields the histone from aberrant aggregation with DNA while $Nap1_2$ and Ran^{GTP} work together to facilitate specific release of the histone from Kap114 to the tetrasome.

H2A-H2B transfer from $Nap1_2$•H2A-H2B•Kap114•Ran^{GTP} to nucleosome

To explore how Kap114, $Nap1_2$, and Ran^{GTP} cooperate in transferring H2A-H2B onto assembling nucleosomes, we used a

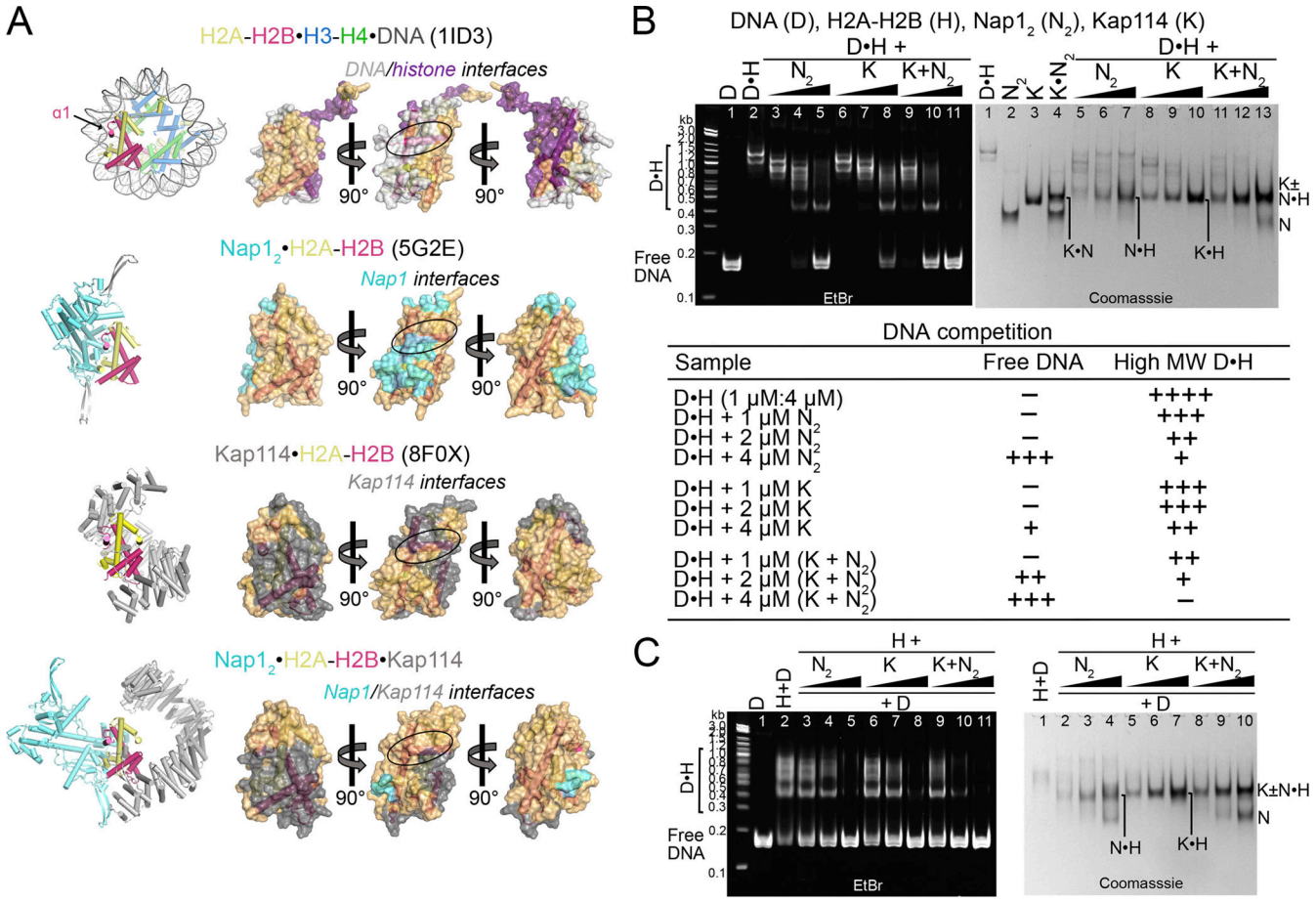

Figure 4. **Kap114 and Nap1$_2$ co-chaperone H2A-H2B in the absence of Ran^{GTP}. (A)** Left, top to bottom: Structures of the nucleosome (1ID3), Nap1$_2$•H2A-H2B (5G2E), Kap114•H2A-H2B (8F0X), and Nap1$_2$•H2A-H2B•Kap114. Right panels, top to bottom: three views of the semi-transparent H2A-H2B surface with cartoon representation underneath, for the corresponding structures in the left panel. Binding interfaces (PDBePISA) are colored according to binding partners. Ovals highlight the H2B α1 helix, which is buried by Nap1$_2$ in Nap1$_2$•H2A-H2B and by Kap114 in Kap114•H2A-H2B, and very likely restricted in access by Nap1$_2$ in Nap1$_2$•H2A-H2B•Kap114. **(B)** DNA competition assays of DNA•H2A-H2B complex (D•H) added to Nap1 (N$_2$), Kap114 (K), or Kap114+Nap1$_2$ mixture (K+N$_2$), in the absence of Ran^{GTP}. Summary of DNA competition assay results as shown below. Samples were visualized using ethidium bromide- and Coomassie-stained native PAGE gels. **(C)** Similar assay as in B, but all proteins were assembled in complexes before the addition of DNA. Source data are available for this figure: SourceData F4.

Kap114 mutant that cannot bind Nap1$_2$. We performed pull-down binding assays with equimolar amounts of Kap114 Δh19L, Nap1$_2$, H2A-H2B, and Ran^{GTP} (Fig. 3 B). Despite its inability to bind Nap1$_2$, the Kap114 Δh19L mutant successfully captured H2A-H2B in the presence of Nap1$_2$, forming a Kap114 Δh19L•H2A-H2B complex, consistent with H2A-H2B's high affinity for the importin (Fig. 3 B) (Jiou et al., 2023). Additionally, Kap114 Δh19L also pulled down H2A-H2B in the presence of Ran^{GTP}, forming the Ran^{GTP}•Kap114 Δh19L•H2A-H2B complex (Fig. 3 B). However, when both Ran^{GTP} and Nap1$_2$ were present, Kap114 Δh19L failed to capture H2A-H2B, suggesting that Ran^{GTP} enabled free Nap1, which cannot bind Kap114 Δh19L, to displace the histone from the importin. These findings imply that in the Nap1$_2$•H2A-H2B•Kap114•Ran^{GTP} complex, Ran^{GTP} may facilitate the transfer of H2A-H2B from Kap114 to Nap1$_2$, optimizing its deposition into nucleosomes (Fig. 6 C). This quaternary assembly likely provides a targeted pathway to efficiently transfer H2A-H2B from Kap114 to Nap1$_2$ to the tetrasome, while minimizing the risk of non-specific or aberrant interactions in the nucleus.

Discussion

We have revealed the structure of the Nap1$_2$•H2A-H2B•Kap114•Ran^{GTP} quaternary complex, which represents the nuclear state of the co-import complex of Nap1$_2$ and H2A-H2B with their importer Kap114. A similar structural arrangement of the ternary Nap1$_2$•H2A-H2B•Kap114 complex suggests that it is the cytoplasmic import complex. In both structures, the DNA-binding surfaces of H2A-H2B are shielded by either Kap114 or Nap1$_2$, consistent with Kap114 and Nap1$_2$ co-chaperoning H2A-H2B, preventing aberrant interactions. Nap1$_2$ in the quaternary/nuclear Nap1$_2$•H2A-H2B•Kap114•Ran^{GTP} complex is essential for chaperoning H2A-H2B in the presence of Ran^{GTP}. The assembly efficiently deposits H2A-H2B into nucleosomes.

Nap1 is mostly cytoplasmic at a steady state (Kellogg et al., 1995), but the Pemberton group showed that it shuttles between the nucleus and the cytoplasm (Mosammaparast et al., 2002). They also identified Nap1 as a cofactor in Kap114-mediated nuclear import of H2A-H2B and revealed its roles in chromatin assembly, transcription elongation, and mRNP biogenesis

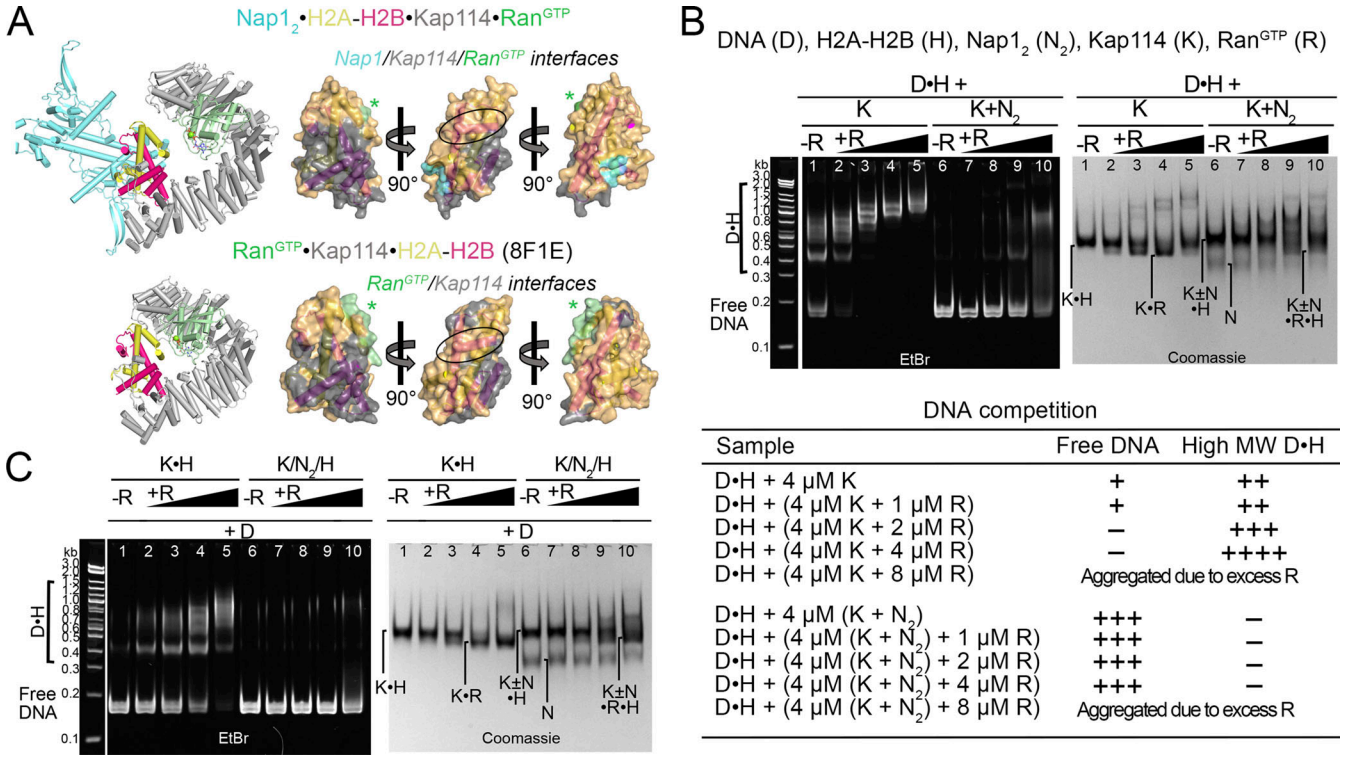

DNA competition

Sample	Free DNA	High MW D•H
D•H + 4 μM K	+	++
D•H + (4 μM K + 1 μM R)	+	++
D•H + (4 μM K + 2 μM R)	–	+++
D•H + (4 μM K + 4 μM R)	–	++++
D•H + (4 μM K + 8 μM R)	Aggregated due to excess R	
D•H + 4 μM (K + N$_2$)	+++	–
D•H + (4 μM (K + N$_2$) + 1 μM R)	+++	–
D•H + (4 μM (K + N$_2$) + 2 μM R)	+++	–
D•H + (4 μM (K + N$_2$) + 4 μM R)	+++	–
D•H + (4 μM (K + N$_2$) + 8 μM R)	Aggregated due to excess R	

Figure 5. **Kap114 and Nap1$_2$ co-chaperone H2A-H2B in the presence of Ran^{GTP}. (A)** Depicted as in Fig. 4 A, histone interaction interfaces in Nap1$_2$•H2A-H2B•Kap114•Ran^{GTP} and Ran^{GTP}•Kap114•H2A-H2B (8F1E). The green asterisks (*) indicate transient Ran^{GTP}-H2A-H2B contacts. H2B α1 (black oval) is likely inaccessible due to the proximity of Nap1$_2$ in Nap1$_2$•H2A-H2B•Kap114•Ran^{GTP} just like Nap1$_2$•H2A-H2B•Kap114; however, it is exposed in Ran^{GTP}•Kap114•H2A-H2B, likely explaining why histone is not effectively chaperoned in this complex. **(B)** DNA competition assays of DNA•H2A-H2B complex (D•H; 1 μM:4 μM) added to Kap114 (K) or Kap114+Nap1$_2$ mixture (K+N$_2$), with a titration of Ran^{GTP} (concentrations indicated in the table of summary of results below. Samples were visualized using ethidium bromide- and Coomassie-stained native PAGE gels. **(C)** Similar assay as in B, but all proteins were assembled in complexes before the addition of DNA. Source data are available for this figure: SourceData F5.

within the nucleus, that others also reported (Aguilar-Gurrieri et al., 2016; Altman and Kellogg, 1997; Andrews et al., 2010; Chen et al., 2016; Del Rosario and Pemberton, 2008; Dronamraju et al., 2017; Hsu et al., 2019; Kellogg and Murray, 1995; Krajewski, 2020; Levchenko and Jackson, 2004; Mazurkiewicz et al., 2006; Moshkin et al., 2013; Nagae et al., 2023; Park et al., 2005; Sharma and Nyborg, 2008; Vlijm et al., 2012). In addition to its well-established role in nucleosome assembly/remodeling, Nap1 also participates in DNA repair (Fan et al., 2024; Gao et al., 2012; Liu et al., 2009; Machida et al., 2014). The Pemberton group further demonstrated direct interactions between Nap1, Kap114, H2A, and H2B, both in the absence and presence of Ran^{GTP} (Mosammaparast et al., 2002). Over two decades later, we now explain these interactions in the context of nuclear import, histone chaperoning, and nucleosome assembly.

Kap114/IMP9 binds H2A-H2B with extremely high affinity in the sub-nanomolar range (Jiou et al., 2023; Shaffer et al., 2023). This strong interaction aligns with the inhibitory effect of Kap114 on nucleosome assembly, as demonstrated here in Fig. 6 and our previous work (Jiou et al., 2023). In the nuclear Nap1$_2$•H2A-H2B•Kap114•Ran^{GTP} complex, the presence of Nap1$_2$ and Ran^{GTP} modulates H2A-H2B affinity, facilitating histone transfer to the assembling nucleosome or another histone chaperone. This targeted release of nuclear import cargo from Kap114 was previously suggested by Pemberton and colleagues who observed that the Ran^{GTP}-mediated release of another cargo, the transcription factor TATA-binding protein (TBP), from Kap114 is enhanced by the presence of TATA-containing double-stranded DNA (Pemberton et al., 1999). Similar to the very high-affinity Kap114-H2A-H2B interaction, Kap114 also binds TBP with a very tight K_D of 1 nM or less (Liao et al., 2020), necessitating both Ran^{GTP} and its nuclear target for efficient cargo release.

Although Ran^{GTP} cannot efficiently dissociate the Kap114-TBP complex, no ternary Ran^{GTP}•Kap114•TBP complex has been reported (Liao et al., 2020; Pemberton et al., 1999). This contrasts with the stable Nap1$_2$•H2A-H2B•Kap114•Ran^{GTP} complex characterized in this study, which can be explained by the distinct cargo binding modes of Kap114. TBP binds in a region separate from the H2A-H2B binding site, interacting with a contiguous surface on the Kap114 solenoid that spans repeat h9-h13, along with contributions from the h8loop and the h19loop—overlapping with the Ran^{GTP} binding site (Liao et al., 2023). In contrast, the H2A-H2B binding site largely does not overlap with that of Ran^{GTP}, and conformational changes in the flexible Kap114 enable simultaneous binding of both the histone and GTPase.

The very tight Kap114–TBP interaction likely contributes to Kap114's ability to regulate TBP-dependent transcription in yeast by sequestering the transcription factor away from promoters

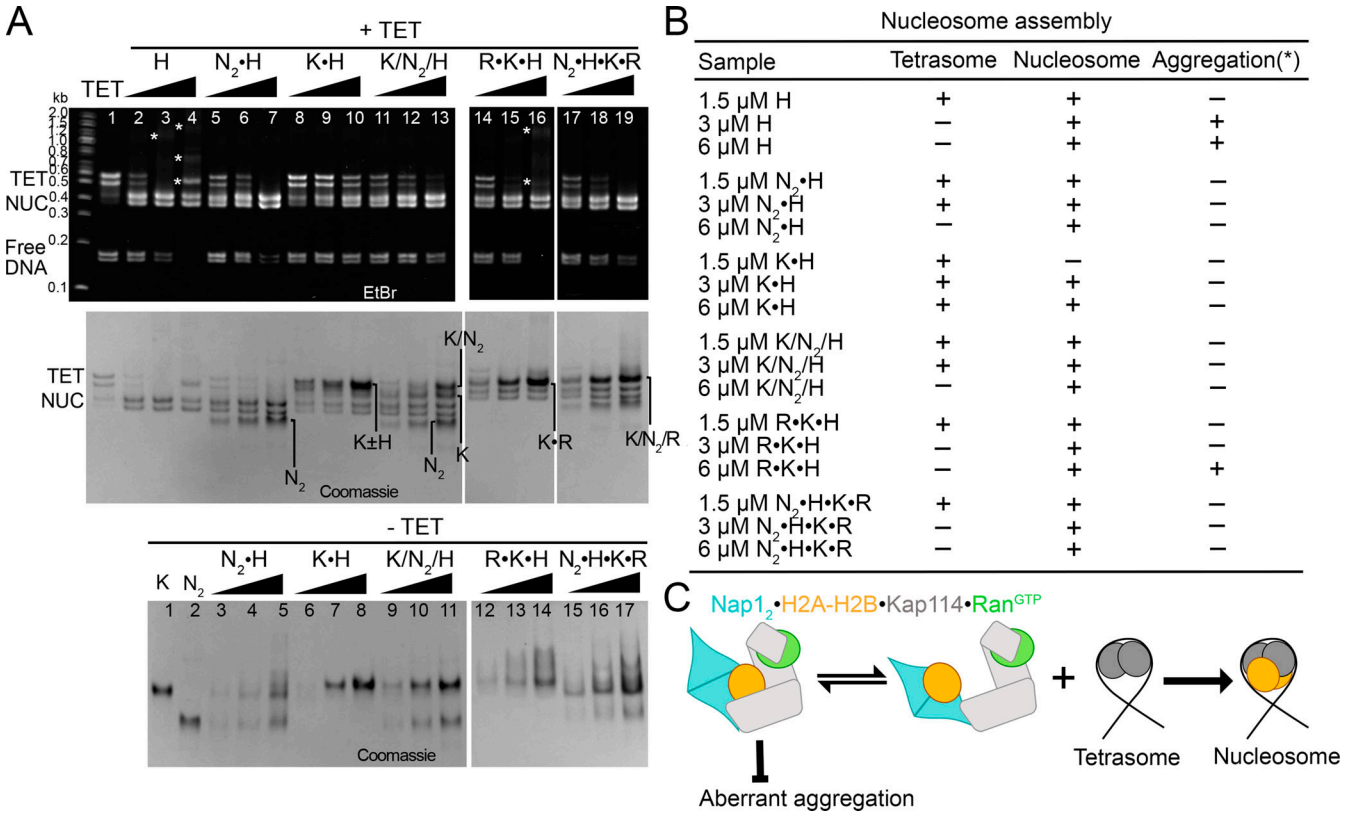

Figure 6. **$Nap1_2$•H2A-H2B•Kap114•Ran^{GTP} effectively deposits H2A-H2B on tetrasomes. (A)** Nucleosome assembly assay: H2A-H2B (H) pre-mixed with increasing concentrations of $Nap1_2$ (N_2) and/or Kap114 (K), without and with Ran^{GTP} (R), before the addition of ~3–4 μM tetrasomes (TET; see Materials and methods). Samples were visualized using ethidium bromide- (top) and Coomassie-stained (middle) native PAGE gels. $Nap1_2$ allows nucleosome (NUC) formation while Kap114 inhibits it. Both Ran^{GTP}•Kap114•H2A-H2B and $Nap1_2$•H2A-H2B•Kap114•Ran^{GTP} form NUC effectively, but the former do not shield H2A-H2B from aggregation with DNA (white asterisks*). Bottom gel: control samples were without TET, where increasing the protein concentration did not affect mobility, indicating that protein complexes were stably formed at 1.5 μM. **(B)** Summary of protein concentrations and nucleosome assembly results. **(C)** Hypothetical model of how $Nap1_2$•H2A-H2B•Kap114•Ran^{GTP} promotes H2A-H2B transfer from Kap114 to assembling nucleosomes. The quaternary complex remains an effective chaperone of H2A-H2B and shields the bound histone from aberrant aggregation while the Kap114-bound Ran^{GTP} likely promotes histone release to the Kap114-bound $Nap1_2$, which can then effectively transfer H2A-H2B to tetrasomes to form nucleosomes. Source data are available for this figure: SourceData F6.

(Liao et al., 2023). Similarly, the unusually strong Kap114–H2A–H2B interaction and the stability of the $Nap1_2$•H2A-H2B•Kap114•Ran^{GTP} complex suggest a potential nuclear role for Kap114. This raises the possibility that Kap114 is involved in chromatin dynamics beyond simply delivering H2A-H2B to assembling the nucleosome. Our study elucidates the latter process, explaining how $Nap1_2$ acts as a co-factor in Kap114-mediated H2A-H2B nuclear import, demonstrating how the importin and histone chaperone function together as co-chaperones.

The collaborative action of Kap114, $Nap1_2$, and Ran^{GTP} could enable precise, efficient, and seamless transfer of H2A-H2B into assembling nucleosomes. Whether such localized release in cells is a more general property of importins is tempting to speculate and has been proposed but the data demonstrating this activity for other importins has not proven conclusive (Lee and Aitchison, 1999). Nonetheless, in the case of Kap114, we have provided valuable mechanistic insight into how nuclear import is tightly coordinated with the targeted release of cargo at its specific nuclear destination to ensure efficiency and mitigate deleterious effects of non-productive interactions.

Materials and methods

Protein constructs, expression, and purification

Kap114 was previously cloned into vector pGEX-4T3 (Cytiva) and subcloned into pMalE (New England BioLabs) using Sal1 and Not1 cut sites. pGEX-4T3 was modified with a TEV cleavage site between the GST tag and Kap114 whereas pMalE was modified with a His_6-tag immediately N-terminus of MBP and a TEV cleavage site after the MBP. Mutant proteins were generated by site-directed mutagenesis or blunt-end ligations with primers and oligos listed in Table S2.

MBP-Kap114 was expressed in BL21 Gold cells grown in LB media, and protein expression was induced with 0.5 mM IPTG for 17 h at 18°C. Cells were harvested by centrifugation at 4,000 *g* (Sorvall BP6) and resuspended in lysis buffer containing 50 mM HEPES 7.0, 150 mM NaCl, 10% (vol/vol) glycerol, 5 mM DTT, 1 mM benzamidine, 10 μg/ml leupeptin, and 50 μg/ml AEBSF,

and frozen. Thawed bacteria cells were lyzed using Emulsiflex homogenizer, the lysate was clarified by centrifugation at 48,400 *g* for 40 min at 4°C (Sorvall RC6), and the supernatant was added to amylose beads (New England Biolabs). The beads were briefly washed with lysis buffer with NaCl added to 300 mM. MBP-Kap114 was then eluted with buffer containing 50 mM HEPES 7.0, 50 mM NaCl, 10% (vol/vol) glycerol, 20 mM maltose, and 2 mM DTT and further purified by ion exchange using HiTrap Q HP column (Cytiva) in 25 mM Bis-Tris, pH 6.5, 0–1 M NaCl, 10% (vol/vol) glycerol, 2 mM DTT. MBP-Kap114 was subjected to a last purification step over SEC using a HiLoad Superdex 200 column (Cytiva) in Assay Buffer containing 20 mM HEPES, pH 7.4, 150 mM NaCl, 2 mM $MgCl_2$, 10% (vol/vol) glycerol, and 2 mM DTT. GST-Kap114 proteins were expressed and purified as previously described (Jiou et al., 2023). In brief, the protocol is similar to the MBP-Kap114 purification described above, with lysis buffer containing 20 mM Tris-HCl, pH 7.5, 1 M NaCl, 15% (vol/vol) glycerol, 2 mM DTT, but purified with Glutathione Sepharose 4B beads (Cytiva). TEV cleavage was performed on a column and proteins were purified by SEC.

Nap1 FL (C200A, C249A, C272A mutation for specific labeling on 414C) cloned into a pHAT4 vector was a gift from Sheena D'Arcy. Nap1 mutants were generated by site-directed mutagenesis using Phusion polymerase (Thermo Fisher Scientific) or CloneAmp HiFi PCR premix (Takara Bio) with primers listed in Table S2. Nap1 FL (WT and mutants) were expressed in BL21 gold cells grown in 2X YT media, and protein expression was induced by 0.5 mM IPTG for 17 h at 18°C. Cells were harvested by centrifugation and resuspended in Nap1 lysis buffer containing 20 mM Tris, pH 7.5, 1 M NaCl, 15% (vol/vol) glycerol, 1 mM DTT, 1 mM benzamidine, 10 µg/ml leupeptin, and 50 µg/ml AEBSF. Thawed cells were lysed, and the clarified lysate was supplemented with 5 mM imidazole at pH 7.8 and added to Ni-NTA agarose (Qiagen), which was washed with the Nap1 lysis buffer with 5 mM imidazole, pH 7.8. The beads were further washed with a buffer containing 20 mM HEPES, pH 7.4, 300 mM NaCl, 15% (vol/vol) glycerol, 1 mM 2-mercaptoethanol with 25 mM imidazole, pH 7.8. Bound protein was eluted with the same buffer supplemented to 250 mM imidazole and concentrated to ~10 ml. 1 mg of TEV protease (purified in-house) was then added to the concentrated protein, overnight, at 4°C. The protein mixture was diluted and passed through Ni-NTA beads to remove TEV and the His tag. Nap1 is further purified using HiTrap Q and Superdex S200.

Nap1 core (residues 75–365), cloned into a pET15b vector, was a gift from Karolin Luger. His-Nap1 core proteins were expressed and purified as previously described (Sarkar et al., 2020). In brief, His-Nap1 core was purified by nickel-NTA affinity and ion exchange chromatography, followed by SEC. For pull-down assays, thrombin (Cat #T4648; Sigma-Aldrich) cleavage was performed overnight at 4°C to remove the His-tag and untagged protein purified by SEC (Superdex S200 increase column [Cytiva]) in Assay Buffer.

Lyophilized *Sc* and *Xl* histones were obtained from "The Histone Source" and refolded according to established protocol (Luger et al., 1997). In brief, 4 mg of each histone was resuspended in 4 ml of unfolding buffer (7 M guanidinium HCL, 20 mM Tris-HCl, pH 7.5, and 10 mM DTT), and incubated at room temperature for 1 h. H2A and H2B, or H3 and H4, were then mixed with extra unfolding buffer to a total of 8–10 ml and incubated at room temp for another 30 min followed by dialysis with 4 liters of cold refolding buffer (2 M NaCl, 10 mM Tris-HCl, pH 7.5, 1 mM EDTA, pH 8.0, and 5 mM β-mercaptoetanol) at 4°C overnight. Refolded histones were then concentrated and purified by SEC using a HiLoad 16/600 Superdex 200 column (Cytiva) pre-equilibrated with refolding buffer. All assays in this paper were performed with *Sc* H2A-H2B unless otherwise stated (Fig. S1 E and Fig. S2 A).

Sc Ran^{GTP} (Gsp1 residues 1–179, with Q71L mutation to stabilize the GTP bound state) is expressed and purified in a pET21d vector as described previously with the addition of a TEV cleavage step (Fung and Chook, 2022). Briefly, Ran was expressed in BL21 gold cells, induced with 0.5 mM IPTG for 12 h at 20°C. Cells were resuspended in buffer containing 50 mM HEPES, pH 7.4, 2 mM MgOAc, 200 mM NaCl, 10 % (vol/vol) glycerol, 5 mM imidazole, pH 7.8, 2 mM 2-mercaptoethanol, 1 mM benzamidine, 10 µg/ml leupeptin, and 50 µg/ml AEBSF. Thawed cells were lysed, and the clarified lysate was incubated with Ni-NTA beads, which were washed. Ran was eluted with buffer containing 50 mM HEPES, pH 7.4, 2 mM MgOAc, 50 mM NaCl, 10% (vol/vol) glycerol, 250 mM imidazole, pH 7.8, and 2 mM 2-mercaptoethanol, concentrated, and treated with 1 mg of TEV overnight incubation at 4°C. TEV-cleaved Ran^{GTP} was purified by ion exchange using HiTrap SP HP column (Cytiva) in buffer containing 20 mM HEPES, pH 7.4, 0–1 M NaCl, 4 mM MgOAc, 10% (vol/vol) glycerol, and clean protein was flash-frozen and stored at −80°C. Ran^{GTP} activity was verified through binding assays with various importins that GTP is bound in the purified Ran, and no additional GTP loading steps were needed.

Pull-down binding assays

All biochemical and biophysical studies were conducted at an ionic strength close to physiological salt levels of 150 mM NaCl. In vitro pull-down binding assays were performed in triplicate by incubating proteins at their indicated concentrations with 20 µl amylose resin (bead bed volume; New England Biolabs) in a 200 µl reaction in Assay Buffer (20 mM HEPES, pH 7.4, 150 mM NaCl, 2 mM $MgCl_2$, 10% (vol/vol) glycerol and 2 mM DTT) for 30 min at 4°C, followed by washing with 500 µl buffer twice. Bound proteins were separated and visualized by SDS-PAGE and Coomassie Blue staining. All gels were imaged in ChemiDoc MP imaging system (Bio-rad). Nap1 band intensities were quantified using Bio-rad Image Lab software, adjusted for the intensity of the MBP-Kap114 band, and normalized to Nap1 WT control. Unpaired, two-sided Student's *t* test was performed. Data distribution was assumed to be normal, but it was not formally tested.

Analytical ultracentrifugation

Individual proteins were dialyzed overnight into AUC buffer containing 20 mM Tris-HCl, pH 7.5, 150 mM NaCl, 2 mM $MgCl_2$ and 2 mM TCEP, at 4°C and assembled in the AUC sample chamber at the indicated concentrations in 400 µl. Sedimentation coefficients were measured by monitoring absorbance at

280 nm in a Beckman-Coulter Optima XL-1 Analytical Ultracentrifuge. Time stamps were corrected using REDATE (Zhao et al., 2013). SEDNTERP was used to calculate the buffer density, buffer viscosity, and protein partial-specific volumes (Laue et al., 1992). SEDFIT was used to calculate sedimentation coefficient distributions c(*s*) where the regularization calculated a confidence level of 0.68 was used, time-independent noise elements were accounted for, and at a resolution of 100 (Schuck, 2000). SEDFIT was also used to estimate molecular weight by obtaining the sedimentation coefficient through integration of c(*s*) and the frictional ratios by refining the fit of the model. The c(*s*) distribution and isotherm integration was done with GUSSI (Brautigam, 2015). Further isotherm fitting was performed using SEDPHAT (Zhao et al., 2015).

Size exclusion chromatography multi-angle light scattering

SEC-MALS experiments were performed in Assay buffer without glycerol with proteins at the indicated molar ratios to 80 µM Kap114 following established protocol, including sample dialysis and buffer filtration (Sarkar et al., 2020). The concentration of proteins is high in the small injection of 100 µl to ensure complete complex formation when it is diluted in the SEC column. The data was collected and processed using ASTRA software using default settings with no de-spiking (Wyatt Technology). The run for 80 µM Kap114 + 80 µM H2A-H2B + 80 µM $Nap1_2$ was interrupted at the void volume due to fractionation issues causing a total pause of 1.895 min. A correction of 1.38933 ml was applied to match other runs.

Cryo-EM sample preparation and data collection and analysis

It is thought that $Nap1_2$•H2A-H2B complex likely forms in the cytoplasm before encountering Kap114 (Bernardes and Chook, 2020; Campos et al., 2010). Therefore, we prepared a cryo-EM sample by first assembling $Nap1_2$ core•H2A-H2B in the presence of excess histones to ensure binding, and then adding Kap114, before subjecting the sample to mild crosslinking. *Sc* H2A-H2B, Nap1 core, and Kap114 were dialyzed separately overnight into cryo-EM buffer containing 20 mM Tris, pH 7.5, 150 mM NaCl, and 2 mM DTT. A 1:2 M ratio mixture of Nap1 core dimer:H2A-H2B was incubated at room temperature for 10 min followed by the addition of 1 M ratio of Kap114, followed by rapid addition of glutaraldehyde to a final concentration of 0.05%. Crosslinking proceeded for 1 min before quenching and removal of glutaraldehyde by SEC using a Superdex 200 10/300 Increase column that was equilibrated with cryo-EM buffer containing TCEP (instead of DTT). 0.5 ml fractions were collected for mass photometry (MP) analysis (details below).

To assemble the Ran^{GTP}/Kap114/Nap1/H2A-H2B complex, a 10 mg/ml mix of a stoichiometric molar ratio of 1 Kap114 to 1 H2A-H2B to 2 $Nap1_2$ FL (His tag intact) to 1 Ran^{GTP} was dialyzed overnight before crosslinking with 0.05% glutaraldehyde for 1 min and separation by SEC in Assay buffer without glycerol. Fractions of 0.25 ml were collected for MP analysis. Fractions with the least aggregated species and most enriched with the relevant complexes (Figs. S2 and S3) were selected for grid preparation.

For Kap114/H2A-H2B/Nap1, the sample was diluted to ∼1.2 mg/ml and supplemented with 0.003125% (wt/vol) Triton X-100. For Ran^{GTP}/Kap114/Nap1/H2A-H2B, the sample was diluted to a ∼1.5 mg/ml with 0.003125% (wt/vol) Tyloxapol. Quantifoil grids were glow-discharged, blotted, and plunge-frozen. Grids were screened and data was collected and analyzed as described below.

Mass photometry for cryo-EM samples

All protein fractions were analyzed using a Refeyn TwoMP Mass Photometer. The laser was warmed up for an hour before use. During that waiting period, the glass slide was washed by alternating between Milli-Q filtered water, isopropanol, and then Milli-Q water, twice. A 2 by 4 strip of wells was adhered to the middle of the glass slide. Immersion oil was applied to the lens before placing the glass slide on top. Prior to the measurement, 2 mg/ml BSA was diluted 100-fold with freshly filtered buffer from the buffer used in S200 of the cryo-EM complex. BSA was used for generating the calibration curve, using an additional 10-fold dilution: we first added 16.2 µl of buffer into a well and brought it to focus then mixed in 1.8 µl of BSA and 60 s movies were recorded. Fractions were diluted to under 7,000 counts for collection in a similar manner as the BSA. Data were processed through Gaussian fitting to provide the peak mass and relative populations using the Refeyn analysis software.

Cryo-EM data collection

A 48-h data collection with the best grid of the Kap114/H2A-H2B/Nap1 core complex was performed at the UT Southwestern Cryo-Electron Microscopy Facility (CEMF) on a Titan Krios microscope (Thermo Fisher Scientific) at 300 kV with a Gatan K3 detector in correlated double sampling super-resolution mode at a magnification of 105,000X corresponding to a pixel size of 0.415 Å. A total of 10,806 movies were collected; each movie was recorded for a total of 60 frames over 5.4 s with an exposure rate of 7.8 electrons/pixel/s. The datasets were collected using SerialEM software (Mastronarde, 2005) with a defocus range of −0.9 and −2.4 µm.

A 24-h data collection was performed on the best grid with Kap114/H2A-H2B/Nap1 FL/Ran^{GTP} complex at the UTSW CEMF on a Titan Krios 300 kV microscope equipped with a Falcon 4i detector at a magnification of 165,000X at pixel size of 0.738 Å with defocus range of −0.9 to −2.2 µm. A total of 9,331 movies were recorded for a total of 1,114 frames over 3.6 s with an exposure rate of ∼8 electrons/pixel/s.

Cryo-EM data processing

Cryo-EM data for the Kap114/H2A-H2B/Nap1 core complex was processed using cryoSPARC version 3 (Punjani et al., 2017). The movies were subjected to Patch Motion Correction (binned twice) and Patch CTF Estimation. Training particles were obtained by blob picking on 100 micrographs and followed by 2D classification of the particle stack. Particles containing Kap114 were used to train on Topaz (Bepler et al., 2019), which picked 665,443 particles. These particles were subjected to three rounds of 2D classification (300 classes/run). 113,471 particles that contained both Kap114 and Nap1 were split into two Ab-initio classes, the $Nap1_2$•H2A-H2B•Kap114 and $Nap1_2$•Kap114•H2A-H2B, and further classified using Heterogenous Refinement.

54,170 particles of $Nap1_2$•H2A-H2B•Kap114 and 59,310 particles of $Nap1_2$•Kap114•H2A-H2B were further refined using Non-Uniform (NU) Refinement resulting in 4.02 and 3.65 Å maps, respectively. To obtain more particles, these maps were used to generate templates for additional template picking on cryoSPARC. This resulted in 4,314,112 total particles that contained $Nap1_2$ only, Kap114•H2A-H2B, $Nap1_2$•H2A-H2B•Kap114, and $Nap1_2$•Kap114•H2A-H2B. After the first round of 2D classification ~1 million particles were further processed for Nap1 core dimer, and another ~1 million particles were further processed for the Kap114-containing complexes. Both Nap1 and Kap114 complexes underwent three more rounds of additional 2D classifications to obtain 468,627 and 675,417 particles, respectively. Two ab initio classes were generated for Nap1 particles and four ab initio classes were generated for the Kap114 complexes followed by classification with heterogeneous refinement. 230,210 Nap1 particles were used in NU Refinement resulting in the final map with 3.2 Å resolution. The $Nap1_2$•H2A-H2B•Kap114 and $Nap1_2$•Kap114•H2A-H2B particles obtained from Topaz were merged with ones obtained from template picking. Duplicates were then removed, resulting in 136,011 $Nap1_2$•H2A-H2B•Kap114 and 148,410 $Nap1_2$•Kap114•H2A-H2B final particles that were used for reconstruction in Non-uniform (NU) refinement with default parameters to obtain maps with 3.5 and 3.2 Å, respectively. Local refinement was performed using a custom fulcrum position at the center of h19 helices, determined in ChimeraX, to obtain improved maps for Nap1 in both reconstructions. Additionally, for $Nap1_2$•Kap114•H2A-H2B map, pose/shift Gaussian prior to alignment was used.

Cryo-EM data for the Kap114/H2A-H2B/Nap1 FL/Ran^{GTP} complex was processed using cryoSPARC version 4.3. The movies were subjected to Patch Motion Correction (no binning) and Patch CTF Estimation. Blob picking on all of the micrographs yielded 2,567,783 initial particles, which was followed by five rounds of 2D classification to 306,757 particles, which were submitted to ab initio reconstruction and hetero-refinement to obtain four classes. Two classes containing Kap114 bound to Ran^{GTP} were used as training particles for Topaz to pick 1,381,753 particles, which were cleaned by three rounds of 2D classification to 358,680 particles. These particles were submitted to ab initio reconstruction and hetero-refinement to obtain four classes, one of which was used for further local CTF refinement and NU refinement with default parameters to obtain a map with 2.9 Å refinement. Density for $Nap1_2$ and H2A-H2B was present in hetero-refinement map and early iterations for NU refinement, but not in the final map. Therefore, a mask was generated using a $Nap1_2$•H2A-H2B•Kap114 docked onto the low-resolution map, and local refinement was performed with default parameters. Directional FSCs were generated using 3DFSC server (Tan et al., 2017).

Structure building/modeling

The initial Nap1 model generated with AlphaFold-Multimer was used to build into the cryo-EM structure of the $Nap1_2$ (Evans et al., 2022, *Preprint*). The initial models used to build the $Nap1_2$•Kap114•H2A-H2B structure included Kap114•H2A-H2B (PDB:8F0X), the Alpha-Fold model of Kap114 (AF-P53067-F1), and our cryo-EM structure of the Nap1 dimer. The $Nap1_2$•H2A-H2B•Kap114 was built using the Ran^{GTP}•H2A-H2B•Kap114 cryo-EM structure (PDB: 8F1E), AF-P53067-F1, and our cryo-EM model of the Nap1 dimer as initial models. The $Nap1_2$•H2A-H2B•Kap114•Ran^{GTP} structure was built using the $Nap1_2$•H2A-H2B•Kap114 cryo-EM structure determined in this study and the Ran^{GTP}•H2A-H2B•Kap114 (PDB: 8F1E) (Jiou et al., 2023). All initial models were roughly docked into the map using UCSF Chimera or ChimeraX (Pettersen et al., 2004, 2021) and then subjected to real-space refinement with global minimization and rigid body restraints in Phenix (Adams et al., 2010). The resulting structures were then manually rebuilt and refined using Coot (Emsley, 2018), further corrected using ISOLDE (Croll, 2018) on UCSF ChimeraX, and subjected to the last round of refinement in Phenix. We used PDBe PISA to calculate solvent-accessible surface areas (Krissinel and Henrick, 2007). We also used PyMOL version 2.5 and the APBS electrostatic plugin for 3D structure and electrostatic analysis (Jurrus et al., 2018; PyMOL, 2020).

Fluorescence polarization

To generate fluorescently labeled Nap1 FL, the proteins were treated with 1 mM DTT for 30 min at room temperature and buffer-exchanged into 20 mM HEPES, pH 7.4, 500 mM NaCl, 10% (vol/vol) glycerol using a HiTrap Desalting column (Cytiva). 4 M excess XFD488 (ATT Bioquest) was added and reaction incubated for 2 h at room temperature in the dark before removal of excess dye by SEC (Superdex S200 increase) in assay buffer. Fluorescence polarization assays were performed in Assay Buffer in triplicates of sixteen 20 µl samples. *Sc* H2A-H2B was serially diluted from 4 µM and mixed with 20 nM labeled $Nap1_2$ proteins in a 1:1 ratio to yield final concentrations in a 384-well black bottom plate (Corning). Measurements were performed in a CLARIOstar Plus plate reader (BMG Labtech) with top optics using excitation filter 482-16, dichroic filter LP 504, and emission filter 530-40; 50 flashes per well. The gain was optimized to target an mP of ~200. Data was analyzed in PALMIST (Scheuermann et al., 2016) and plotted in GUSSI.

DNA competition assays

601 Widom DNA was purified from pUC19-30X601 grown in C2925 dam^-dcm^- cells (gift from Dr. Mike Rosen) using Qiagen Giga prep kit following the manufacturer's protocol. The DNA was resuspended in 10 mM Tris-HCl, pH 7.4, 1 mM EDTA in the last step of purification. EcoRV (New England Biolabs) cleavage was performed in CutSmart buffer overnight and the DNA was extracted using PCIAA and precipitated in sodium acetate, pH 5.2, and ethanol. The DNA was then rinsed with ethanol, dried, and resolubilized in 10 mM Tris-HCl pH7.4, 10 mM $MgCl_2$. The cut insert was separated from the vector using PEG8000 precipitation and subjected to a final ion exchange purification on a DEAE-FF column before it was concentrated and frozen.

DNA was mixed with H2A-H2B, Kap114, and/or $Nap1_2$ FL with and without Ran^{GTP} at the indicated concentrations in 15 µl reactions in assay buffer. DNA was either premixed with H2A-H2B in a 3X concentration master mix or, alternatively, added at the end. Reactions were incubated at room temperature for

30 min and then 5 µl of sample buffer containing 20% (vol/vol) glycerol and bromophenol blue was added. 8 µl each of this gel sample was run on two separate Native 5% PAGE gels with 0.5X TBE at 150 V for 40 min. One gel was stained with EtBr in water and the other with Coomassie Blue. Gels were imaged in Chem-iDoc MP imaging system. Assays were performed in duplicates.

Nucleosome assembly assays

Tetrasomes were made by mixing *Xl* H3-H4 tetramers and DNA at 1:1 ratio (DNA conc = 1 mg/ml) in 10 mM HEPES pH7.4, 1 mM EDTA, 2 M NaCl, 1 mM DTT and then dialyzed step-wise from 2 M NaCl (0.5 h) to 1 M (1 h), 0.85 M (1.5 h), 0.65 M (1.5 h), 0.2 M (1.5 h), and 0.15 NaCl M (overnight) at 4°C. The volume was measured at the end and the reaction was diluted with assay buffer before use, assuming 100% formation of tetrasomes. Master mixes of *Sc* H2A-H2B, Kap114, and $Nap1_2$ FL with or without Ran^{GTP} were assembled and mixed with tetrasomes in 10 µl reactions on ice and incubated at room temperature for 1 h before addition of 4X sample buffer with 20% glycerol. 3 µl of the resulting samples were visualized the same way as DNA competition assays. Assays were performed in duplicates. The input sample in lane 1 of Fig. 6 A shows that tetrasome formation is not 100% complete and free DNA was present. The strongest nucleosome band is observed in lane 7 in Fig. 6 A with 6 µM $Nap1_2$•H2A-H2B, suggesting that the tetrasome concentration was likely ∼3 µM.

Online supplemental material

Fig. S1 shows the biochemical analysis of Kap114, Nap1, and H2A-H2B binary and tertiary interactions. Fig. S2 shows the biochemical analysis of Kap114, Nap1, and H2A-H2B in the presence of Ran^{GTP} and details for cryoEM sample preparation and data analysis for the quaternary complex. Fig. S3 shows cryoEM sample preparation and data analysis for the ternary Kap114/Nap1/H2A-H2B sample. Fig. S4 shows the structural analysis for complexes described in this study and control binding experiment for Nap1 mutants. Table S1 shows cryoEM data collection, refinement, and validation statistics for the Nap1 core and $Nap1_2$•Kap114•H2A-H2B structure. Table S2 contains primers used in this study.

Data availability

The data underlying Figs. 2, S2, and S3 are openly available in PDB/EMDB at 9B3I/EMD-44141, EMD44150, and EMD44151 (Fung et al., 2024a, 2024b, 2024c); 9B31/EMD-44120, EMD-44121, and EMD-44122 (Jiou et al., 2024c); 9B3F/EMD-44136, EMD-44137, and EMD-44140 (Jiou et al., 2024b); and 9B23/EMD-44095 (Jiou et al., 2024a).

Acknowledgments

We thank all members of the Structural Biology Laboratory (SBL) and the CEMF in UTSW for their expert assistance with cryo-EM data collection. We greatly appreciate Macromolecular Biophysics Resource (MBR) and Chad Brautigam for discussion and use of the AUC and Mass Photometer. We also thank the Erzberger lab for using their plate reader for FP assays. We thank Rosen Lab for help with the Widom DNA purification. We also thank Casey Wing, Mike Rosen, and Mike Rout for critical reading of the manuscript, and we acknowledge the use of ChatGPT in condensing and refining texts. We thank the D'Arcy lab for the use of their SEC-MALS equipment and Joy Shaffer for training.

SBL and CEMF at UTSW are partially supported by grant RP220582 from the Cancer Prevention & Research Institute of Texas (CPRIT). The Refeyn Mass Photometer in MBR was supported by grant S10-OD030312 from the National Institute of Health. Molecular graphics and analyses performed with UCSF ChimeraX, developed by the Resource for Biocomputing, Visualization, and Informatics at the University of California, San Francisco, with support from National Institutes of Health R01-GM129325 and the Office of Cyber Infrastructure and Computational Biology, National Institute of Allergy and Infectious Diseases. This research used resources of the Advanced Photon Source, a U.S. Department of Energy (DOE) Office of Science user facility operated for the DOE Office of Science by Argonne National Laboratory under Contract No. DE-AC02-06CH11357. This work was funded by NIGMS of NIH under Awards R35GM141461 (Y.M. Chook), R01GM069909 (Y.M. Chook), T32GM008203 (J. Jiou), the Welch Foundation Grants I-1532 (Y.M. Chook), support from the Alfred and Mabel Gilman Chair in Molecular Pharmacology, Eugene McDermott Scholar in Biomedical Research (Y.M. Chook), and the Gilman Special Opportunities Award (H.Y.J. Fung). Open Access funding provided by The University of Texas Southwestern Medical Center.

Author contributions: H.Y.J. Fung: Data curation, Formal analysis, Investigation, Methodology, Validation, Visualization, Writing - original draft, Writing - review & editing, J. Jiou: Formal analysis, Investigation, Methodology, Resources, Visualization, A.B. Niesman: Investigation, Writing - review & editing, N.E. Bernardes: Investigation, Writing - review & editing, Y.M. Chook: Conceptualization, Data curation, Formal analysis, Funding acquisition, Investigation, Methodology, Project administration, Resources, Supervision, Validation, Visualization, Writing - original draft, Writing - review & editing.

Disclosures: The authors declare no competing interests exist.

Submitted: 26 August 2024
Revised: 1 October 2024
Accepted: 17 October 2024

References

Adams, P.D., P.V. Afonine, G. Bunkóczi, V.B. Chen, I.W. Davis, N. Echols, J.J. Headd, L.W. Hung, G.J. Kapral, R.W. Grosse-Kunstleve, et al. 2010. PHENIX: A comprehensive python-based system for macromolecular structure solution. *Acta Crystallogr. D Biol. Crystallogr.* 66:213–221. https://doi.org/10.1107/S0907444909052925

Aguilar-Gurrieri, C., A. Larabi, V. Vinayachandran, N.A. Patel, K. Yen, R. Reja, I.O. Ebong, G. Schoehn, C.V. Robinson, B.F. Pugh, and D. Panne. 2016. Structural evidence for Nap1-dependent H2A-H2B deposition and nucleosome assembly. *EMBO J.* 35:1465–1482. https://doi.org/10.15252/embj.201694105

Altman, R., and D. Kellogg. 1997. Control of mitotic events by Nap1 and the Gin4 kinase. *J. Cell Biol.* 138:119–130. https://doi.org/10.1083/jcb.138.1.119

Andrews, A.J., X. Chen, A. Zevin, L.A. Stargell, and K. Luger. 2010. The histone chaperone Nap1 promotes nucleosome assembly by eliminating nonnucleosomal histone DNA interactions. *Mol. Cell.* 37:834–842. https://doi.org/10.1016/j.molcel.2010.01.037

Baake, M., D. Doenecke, and W. Albig. 2001. Characterisation of nuclear localisation signals of the four human core histones. *J. Cell. Biochem.* 81:333–346. https://doi.org/10.1002/1097-4644(20010501)81:2<333::AID-JCB1048>3.0.CO;2-D

Benson, L.J., Y. Gu, T. Yakovleva, K. Tong, C. Barrows, C.L. Strack, R.G. Cook, C.A. Mizzen, and A.T. Annunziato. 2006. Modifications of H3 and H4 during chromatin replication, nucleosome assembly, and histone exchange. *J. Biol. Chem.* 281:9287–9296. https://doi.org/10.1074/jbc.M512956200

Bepler, T., A. Morin, M. Rapp, J. Brasch, L. Shapiro, A.J. Noble, and B. Berger. 2019. Positive-unlabeled convolutional neural networks for particle picking in cryo-electron micrographs. *Nat. Methods.* 16:1153–1160. https://doi.org/10.1038/s41592-019-0575-8

Bernardes, N.E., and Y.M. Chook. 2020. Nuclear import of histones. *Biochem. Soc. Trans.* 48:2753–2767. https://doi.org/10.1042/BST20200572

Brautigam, C.A. 2015. Calculations and publication-quality illustrations for analytical ultracentrifugation data. *Methods Enzymol.* 562:109–133. https://doi.org/10.1016/bs.mie.2015.05.001

Calvert, M.E., K.M. Keck, C. Ptak, J. Shabanowitz, D.F. Hunt, and L.F. Pemberton. 2008. Phosphorylation by casein kinase 2 regulates Nap1 localization and function. *Mol. Cell. Biol.* 28:1313–1325. https://doi.org/10.1128/MCB.01035-07

Campos, E.I., J. Fillingham, G. Li, H. Zheng, P. Voigt, W.H. Kuo, H. Seepany, Z. Gao, L.A. Day, J.F. Greenblatt, and D. Reinberg. 2010. The program for processing newly synthesized histones H3.1 and H4. *Nat. Struct. Mol. Biol.* 17:1343–1351. https://doi.org/10.1038/nsmb.1911

Chang, L., S.S. Loranger, C. Mizzen, S.G. Ernst, C.D. Allis, and A.T. Annunziato. 1997. Histones in transit: Cytosolic histone complexes and diacetylation of H4 during nucleosome assembly in human cells. *Biochemistry.* 36:469–480. https://doi.org/10.1021/bi962069i

Chen, X., S. D'Arcy, C.A. Radebaugh, D.D. Krzizike, H.A. Giebler, L. Huang, J.K. Nyborg, K. Luger, and L.A. Stargell. 2016. Histone chaperone Nap1 is a major regulator of histone H2A-H2B dynamics at the inducible GAL locus. *Mol. Cell. Biol.* 36:1287–1296. https://doi.org/10.1128/MCB.00835-15

Croll, T.I. 2018. ISOLDE: A physically realistic environment for model building into low-resolution electron-density maps. *Acta Crystallogr. D Struct. Biol.* 74:519–530. https://doi.org/10.1107/S2059798318002425

Dasso, M. 2002. The Ran GTPase: Theme and variations. *Curr. Biol.* 12: R502–R508. https://doi.org/10.1016/S0960-9822(02)00970-3

Del Rosario, B.C., and L.F. Pemberton. 2008. Nap1 links transcription elongation, chromatin assembly, and messenger RNP complex biogenesis. *Mol. Cell. Biol.* 28:2113–2124. https://doi.org/10.1128/MCB.02136-07

Dronamraju, R., S. Ramachandran, D.K. Jha, A.T. Adams, J.V. DiFiore, M.A. Parra, N.V. Dokholyan, and B.D. Strahl. 2017. Redundant functions for Nap1 and Chz1 in H2A.Z deposition. *Sci. Rep.* 7:10791. https://doi.org/10.1038/s41598-017-11003-8

Elsässer, S.J., and S. D'Arcy. 2013. Towards a mechanism for histone chaperones. *Biochim. Biophys. Acta.* 1819:211–221. https://doi.org/10.1016/j.bbagrm.2011.07.007

Emsley, P. 2018. New tools for ligand refinement and validation in Coot and CCP4. *Acta Crystallogr. A. Found. Adv.* 74:A390. https://doi.org/10.1107/S0108767318096101

Evans, R., M. O'Neill, A. Pritzel, N. Antropova, A. Senior, T. Green, A. Žídek, R. Bates, S. Blackwell, J. Yim, et al. 2022. Protein complex prediction with AlphaFold-Multimer. *bioRxiv* https://doi.org/10.1101/2021.10.04.463034 (Preprint post March 10, 2022).

Fan, T., T. Shi, R. Sui, J. Wang, H. Kang, Y. Yu, and Y. Zhu. 2024. The chromatin remodeler ERCC6 and the histone chaperone NAP1 are involved in apurinic/apyrimidinic endonuclease-mediated DNA repair. *Plant Cell.* 36:2238–2252. https://doi.org/10.1093/plcell/koae052

Fung, H.Y.J., and Y.M. Chook. 2022. Binding affinity measurement of nuclear export signal peptides to their exporter CRM1. *Methods Mol. Biol.* 2502: 245–256. https://doi.org/10.1007/978-1-0716-2337-4_16

Fung, H.Y.J., J. Jiou, and Y.M. Chook. 2024a. Cryo-EM structure of yeast (Nap1)2-H2A-H2B-Kap114-RanGTP. PDB/EMDB. 9B3I/EMD-44141. https://www.ebi.ac.uk/emdb/EMD-44141

Fung, H.Y.J, J Jiou, and Y.M. Chook. 2024b. Local refined map for Nap1 and H2A-H2B region in (Nap1)2-H2A-H2B-Kap114-RanGTP structure. *EMDB*. https://www.ebi.ac.uk/emdb/EMD-44150

Fung, H.Y.J., J Jiou, and Y.M. Chook. 2024c. Consensus volume for (Nap1)2-H2A-H2B-Kap114-RanGTP. *EMDB*. https://www.ebi.ac.uk/emdb/EMD-44151

Gao, J., Y. Zhu, W. Zhou, J. Molinier, A. Dong, and W.H. Shen. 2012. NAP1 family histone chaperones are required for somatic homologous recombination in Arabidopsis. *Plant Cell.* 24:1437–1447. https://doi.org/10.1105/tpc.112.096792

Görlich, D., N. Panté, U. Kutay, U. Aebi, and F.R. Bischoff. 1996. Identification of different roles for RanGDP and RanGTP in nuclear protein import. *EMBO J.* 15:5584–5594. https://doi.org/10.1002/j.1460-2075.1996.tb00943.x

Hahn, S., and G. Schlenstedt. 2011. Importin β-type nuclear transport receptors have distinct binding affinities for Ran-GTP. *Biochem. Biophys. Res. Commun.* 406:383–388. https://doi.org/10.1016/j.bbrc.2011.02.051

Hammond, C.M., C.B. Strømme, H. Huang, D.J. Patel, and A. Groth. 2017. Histone chaperone networks shaping chromatin function. *Nat. Rev. Mol. Cell Biol.* 18:141–158. https://doi.org/10.1038/nrm.2016.159

Hodges, J.L., J.H. Leslie, N. Mosammaparast, Y. Guo, J. Shabanowitz, D.F. Hunt, and L.F. Pemberton. 2005. Nuclear import of TFIIB is mediated by Kap114p, a karyopherin with multiple cargo-binding domains. *Mol. Biol. Cell.* 16:3200–3210. https://doi.org/10.1091/mbc.e04-11-0990

Hogan, A.K., and D.R. Foltz. 2021. Reduce, retain, recycle: Mechanisms for promoting histone protein degradation versus stability and retention. *Mol. Cell. Biol.* 41:e0000721. https://doi.org/10.1128/MCB.00007-21

Hsu, K.W., S.Y. Chow, B.Y. Su, Y.H. Lu, C.J. Chen, W.L. Chen, M.Y. Cheng, and H.F. Fan. 2019. The synergy between RSC, Nap1 and adjacent nucleosome in nucleosome remodeling. *Biochim. Biophys. Acta. Gene Regul. Mech.* 1862:129–140. https://doi.org/10.1016/j.bbagrm.2018.11.008

Huang, Y., Y. Dai, and Z. Zhou. 2020. Mechanistic and structural insights into histone H2A-H2B chaperone in chromatin regulation. *Biochem. J.* 477: 3367–3386. https://doi.org/10.1042/BCJ20190852

Jäkel, S., J.M. Mingot, P. Schwarzmaier, E. Hartmann, and D. Görlich. 2002. Importins fulfil a dual function as nuclear import receptors and cytoplasmic chaperones for exposed basic domains. *EMBO J.* 21:377–386. https://doi.org/10.1093/emboj/21.3.377

Jiou, J., H.Y.J. Fung, and Y.M. Chook. 2024a. Cryo-EM structure of Nap1 core. PDB/EMDB. 9B23/EMD-44095. https://doi.org/10.2210/pdb9B23/pdb

Jiou, J., H.Y.J. Fung, and Y.M. Chook. 2024b. Cryo-EM structure of yeast (Nap1)2-H2A-H2B-Kap114. PDB/EMDB. 9B3F/EMD-44136, Locally refined map for Nap1 and H2A-H2B in (Nap1)2-H2A-H2B-Kap114 structure. EMD-44137 and Consensus volume for (Nap1)2-H2A-H2B-Kap114 structure. EMD-44140. https://doi.org/10.2210/pdb9B3F/pdb

Jiou, J., H.Y.J. Fung, and Y.M. Chook. 2024c. Cryo-EM structure of yeast (Nap1)2-Kap114-H2A-H2B. PDB/EMDB. 9B31/EMD-44120, Local refined map for Nap1 region from (Nap1)2-Kap114-H2A-H2B structure. EMD-44121 and Consensus volume for (Nap1)2-Kap114-H2A-H2B. EMD-44122. https://doi.org/10.2210/pdb9B31/pdb

Jiou, J., J.M. Shaffer, N.E. Bernades, H.Y.J. Fung, J. Kikumoto Dias, S. D'Arcy, and Y.M. Chook. 2023. Mechanism of RanGTP priming H2A-H2B release from Kap114 in an atypical RanGTP • Kap114 • H2A-H2B complex. *Proc. Natl. Acad. Sci. USA.* 120:e2301199120. https://doi.org/10.1073/pnas.2301199120

Johnson-Saliba, M., N.A. Siddon, M.J. Clarkson, D.J. Tremethick, and D.A. Jans. 2000. Distinct importin recognition properties of histones and chromatin assembly factors. *FEBS Lett.* 467:169–174. https://doi.org/10.1016/S0014-5793(00)01142-X

Jurrus, E., D. Engel, K. Star, K. Monson, J. Brandi, L.E. Felberg, D.H. Brookes, L. Wilson, J. Chen, K. Liles, et al. 2018. Improvements to the APBS biomolecular solvation software suite. *Protein Sci.* 27:112–128. https://doi.org/10.1002/pro.3280

Kellogg, D.R., A. Kikuchi, T. Fujii-Nakata, C.W. Turck, and A.W. Murray. 1995. Members of the NAP/SET family of proteins interact specifically with B-type cyclins. *J. Cell Biol.* 130:661–673. https://doi.org/10.1083/jcb.130.3.661

Kellogg, D.R., and A.W. Murray. 1995. NAP1 acts with Clb1 to perform mitotic functions and to suppress polar bud growth in budding yeast. *J. Cell Biol.* 130:675–685. https://doi.org/10.1083/jcb.130.3.675

Kimura, M., Y. Morinaka, K. Imai, S. Kose, P. Horton, and N. Imamoto. 2017. Extensive cargo identification reveals distinct biological roles of the 12 importin pathways. *Elife.* 6:e21184. https://doi.org/10.7554/eLife.21184

Krajewski, W.A. 2020. The intrinsic stability of H2B-ubiquitylated nucleosomes and their in vitro assembly/disassembly by histone chaperone NAP1. *Biochim. Biophys. Acta, Gen. Subj.* 1864:129497. https://doi.org/10.1016/j.bbagen.2019.129497

Krissinel, E., and K. Henrick. 2007. Inference of macromolecular assemblies from crystalline state. *J. Mol. Biol.* 372:774–797. https://doi.org/10.1016/j.jmb.2007.05.022

Laue, T.M., B. Shah, T.M. Ridgeway, and S.L. Pelletier. 1992. Computer-aided interpretation of sedimentation data for proteins. *In* Analytical Ultracentrifugation in Biochemistry and Polymer Science. S.E. Harding, J.C. Horton, and A.J. Rowe, editors. Royal Society of Chemistry, Cambridge, UK. 90–125.

Lee, D.C., and J.D. Aitchison. 1999. Kap104p-mediated nuclear import. Nuclear localization signals in mRNA-binding proteins and the role of Ran

and Rna. *J. Biol. Chem.* 274:29031–29037. https://doi.org/10.1074/jbc.274.41.29031

Levchenko, V., and V. Jackson. 2004. Histone release during transcription: NAP1 forms a complex with H2A and H2B and facilitates a topologically dependent release of H3 and H4 from the nucleosome. *Biochemistry*. 43: 2359–2372. https://doi.org/10.1021/bi035737q

Liao, C.C., S. Shankar, W.C. Pi, C.C. Chang, G.R. Ahmed, W.Y. Chen, and K.C. Hsia. 2020. Karyopherin Kap114p-mediated trans-repression controls ribosomal gene expression under saline stress. *EMBO Rep.* 21:e48324. https://doi.org/10.15252/embr.201948324

Liao, C.C., Y.S. Wang, W.C. Pi, C.H. Wang, Y.M. Wu, W.Y. Chen, and K.C. Hsia. 2023. Structural convergence endows nuclear transport receptor Kap114p with a transcriptional repressor function toward TATA-binding protein. *Nat. Commun.* 14:5518. https://doi.org/10.1038/s41467-023-41206-9

Liu, Z.Q., Y. Zhu, J. Gao, F. Yu, A.W. Dong, and W.H. Shen. 2009. Molecular and reverse genetic characterization of NUCLEOSOME ASSEMBLY PROTEIN1 (NAP1) genes unravels their function in transcription and nucleotide excision repair in transcription and nucleotide excision repair in Arabidopsis thaliana. *Plant J.* 59:27–38. https://doi.org/10.1111/j.1365-313X.2009.03844.x

Luger, K., A.W. Mäder, R.K. Richmond, D.F. Sargent, and T.J. Richmond. 1997. Crystal structure of the nucleosome core particle at 2.8 A resolution. *Nature*. 389:251–260. https://doi.org/10.1038/38444

Machida, S., M. Takaku, M. Ikura, J. Sun, H. Suzuki, W. Kobayashi, A. Kinomura, A. Osakabe, H. Tachiwana, Y. Horikoshi, et al. 2014. Nap1 stimulates homologous recombination by RAD51 and RAD54 in higher-ordered chromatin containing histone H1. *Sci. Rep.* 4:4863. https://doi.org/10.1038/srep04863

Mastronarde, D.N. 2005. Automated electron microscope tomography using robust prediction of specimen movements. *J. Struct. Biol.* 152:36–51. https://doi.org/10.1016/j.jsb.2005.07.007

Mazurkiewicz, J., J.F. Kepert, and K. Rippe. 2006. On the mechanism of nucleosome assembly by histone chaperone NAP1. *J. Biol. Chem.* 281: 16462–16472. https://doi.org/10.1074/jbc.M511619200

Mosammaparast, N., B.C. Del Rosario, and L.F. Pemberton. 2005. Modulation of histone deposition by the karyopherin kap114. *Mol. Cell. Biol.* 25: 1764–1778. https://doi.org/10.1128/MCB.25.5.1764-1778.2005

Mosammaparast, N., C.S. Ewart, and L.F. Pemberton. 2002. A role for nucleosome assembly protein 1 in the nuclear transport of histones H2A and H2B. *EMBO J.* 21:6527–6538. https://doi.org/10.1093/emboj/cdf647

Mosammaparast, N., K.R. Jackson, Y. Guo, C.J. Brame, J. Shabanowitz, D.F. Hunt, and L.F. Pemberton. 2001. Nuclear import of histone H2A and H2B is mediated by a network of karyopherins. *J. Cell Biol.* 153:251–262. https://doi.org/10.1083/jcb.153.2.251

Moshkin, Y.M., C.M. Doyen, T.W. Kan, G.E. Chalkley, K. Sap, K. Bezstarosti, J.A. Demmers, Z. Ozgur, W.F. van Ijcken, and C.P. Verrijzer. 2013. Histone chaperone NAP1 mediates sister chromatid resolution by counteracting protein phosphatase 2A. *PLoS Genet.* 9:e1003719. https://doi.org/10.1371/journal.pgen.1003719

Mühlhäusser, P., E.C. Müller, A. Otto, and U. Kutay. 2001. Multiple pathways contribute to nuclear import of core histones. *EMBO Rep.* 2:690–696. https://doi.org/10.1093/embo-reports/kve168

Nagae, F., S. Takada, and T. Terakawa. 2023. Histone chaperone Nap1 dismantles an H2A/H2B dimer from a partially unwrapped nucleosome. *Nucleic Acids Res.* 51:5351–5363. https://doi.org/10.1093/nar/gkad396

O'Reilly, A.J., J.B. Dacks, and M.C. Field. 2011. Evolution of the karyopherin-β family of nucleocytoplasmic transport factors; ancient origins and continued specialization. *PLoS One*. 6:e19308. https://doi.org/10.1371/journal.pone.0019308

Ohtomo, H., T. Yamane, T. Oda, N. Kodera, J.I. Kurita, Y. Tsunaka, R. Amyot, M. Ikeguchi, and Y. Nishimura. 2023. Dynamic solution structures of whole human NAP1 dimer bound to one and two histone H2A-H2B heterodimers obtained by integrative methods. *J. Mol. Biol.* 435:168189. https://doi.org/10.1016/j.jmb.2023.168189

Okuwaki, M., K. Kato, and K. Nagata. 2010. Functional characterization of human nucleosome assembly protein 1-like proteins as histone chaperones. *Genes Cells*. 15:13–27. https://doi.org/10.1111/j.1365-2443.2009.01361.x

Padavannil, A., P. Sarkar, S.J. Kim, T. Cagatay, J. Jiou, C.A. Brautigam, D.R. Tomchick, A. Sali, S. D'Arcy, and Y.M. Chook. 2019. Importin-9 wraps around the H2A-H2B core to act as nuclear importer and histone chaperone. *Elife*. 8:e43630. https://doi.org/10.7554/eLife.43630

Park, Y.J., J.V. Chodaparambil, Y. Bao, S.J. McBryant, and K. Luger. 2005. Nucleosome assembly protein 1 exchanges histone H2A-H2B dimers and assists nucleosome sliding. *J. Biol. Chem.* 280:1817–1825. https://doi.org/10.1074/jbc.M411347200

Park, Y.J., S.J. McBryant, and K. Luger. 2008. A beta-hairpin comprising the nuclear localization sequence sustains the self-associated states of nucleosome assembly protein 1. *J. Mol. Biol.* 375:1076–1085. https://doi.org/10.1016/j.jmb.2007.11.031

Pemberton, L.F., J.S. Rosenblum, and G. Blobel. 1999. Nuclear import of the TATA-binding protein: Mediation by the karyopherin Kap114p and a possible mechanism for intranuclear targeting. *J. Cell Biol.* 145: 1407–1417. https://doi.org/10.1083/jcb.145.7.1407

Pettersen, E.F., T.D. Goddard, C.C. Huang, G.S. Couch, D.M. Greenblatt, E.C. Meng, and T.E. Ferrin. 2004. UCSF Chimera--a visualization system for exploratory research and analysis. *J. Comput. Chem.* 25:1605–1612. https://doi.org/10.1002/jcc.20084

Pettersen, E.F., T.D. Goddard, C.C. Huang, E.C. Meng, G.S. Couch, T.I. Croll, J.H. Morris, and T.E. Ferrin. 2021. UCSF ChimeraX: Structure visualization for researchers, educators, and developers. *Protein Sci.* 30:70–82. https://doi.org/10.1002/pro.3943

Punjani, A., J.L. Rubinstein, D.J. Fleet, and M.A. Brubaker. 2017. cryoSPARC: algorithms for rapid unsupervised cryo-EM structure determination. *Nat. Methods*. 14:290–296. https://doi.org/10.1038/nmeth.4169

PyMOL. 2020. *The PyMOL Molecular Graphics System, Version 2.5*. Schrödinger, LLC, New York, NY, USA.

Sarkar, P., N. Akhavantabib, and S. D'Arcy. 2020. Comprehensive analysis of histone-binding proteins with multi-angle light scattering. *Methods*. 184:93–101. https://doi.org/10.1016/j.ymeth.2020.01.014

Scheuermann, T.H., S.B. Padrick, K.H. Gardner, and C.A. Brautigam. 2016. On the acquisition and analysis of microscale thermophoresis data. *Anal. Biochem.* 496:79–93. https://doi.org/10.1016/j.ab.2015.12.013

Schuck, P. 2000. Size-distribution analysis of macromolecules by sedimentation velocity ultracentrifugation and lamm equation modeling. *Biophys. J.* 78:1606–1619. https://doi.org/10.1016/S0006-3495(00)76713-0

Schwamborn, K., W. Albig, and D. Doenecke. 1998. The histone H1(0) contains multiple sequence elements for nuclear targeting. *Exp. Cell Res.* 244:206–217. https://doi.org/10.1006/excr.1998.4177

Seidel, M., N. Romanov, A. Obarska-Kosinska, A. Becker, N. Trevisan Doimo de Azevedo, J. Provaznik, S.R. Nagaraja, J.J.M. Landry, V. Benes, and M. Beck. 2023. Co-translational binding of importins to nascent proteins. *Nat. Commun.* 14:3418. https://doi.org/10.1038/s41467-023-39150-9

Shaffer, J.M., J Jiou, K Tripathi, O.S. Olaluwoye, H.Y.J. Fung, Y.M. Chook, and S D'Arcy. 2023. Molecular basis of RanGTP-activated release of Histones H2A-H2B from Importin-9. *Structure*. 31:903–911. https://doi.org/10.1016/j.str.2023.06.001

Sharma, N., and J.K. Nyborg. 2008. The coactivators CBP/p300 and the histone chaperone NAP1 promote transcription-independent nucleosome eviction at the HTLV-1 promoter. *Proc. Natl. Acad. Sci. USA*. 105: 7959–7963. https://doi.org/10.1073/pnas.0800534105

Singh, R.K., D. Liang, U.R. Gajjalaiahvari, M.H. Kabbaj, J. Paik, and A. Gunjan. 2010. Excess histone levels mediate cytotoxicity via multiple mechanisms. *Cell Cycle*. 9:4236–4244. https://doi.org/10.4161/cc.9.20.13636

Straube, K., J.S. Blackwell Jr., and L.F. Pemberton. 2010. Nap1 and Chz1 have separate Htz1 nuclear import and assembly functions. *Traffic*. 11: 185–197. https://doi.org/10.1111/j.1600-0854.2009.001010.x

Tagami, H., D. Ray-Gallet, G. Almouzni, and Y. Nakatani. 2004. Histone H3.1 and H3.3 complexes mediate nucleosome assembly pathways dependent or independent of DNA synthesis. *Cell*. 116:51–61. https://doi.org/10.1016/S0092-8674(03)01064-X

Tan, Y.Z., P.R. Baldwin, J.H. Davis, J.R. Williamson, C.S. Potter, B. Carragher, and D. Lyumkis. 2017. Addressing preferred specimen orientation in single-particle cryo-EM through tilting. *Nat. Methods*. 14:793–796. https://doi.org/10.1038/nmeth.4347

Vlijm, R., J.S. Smitshuijzen, A. Lusser, and C. Dekker. 2012. NAP1-assisted nucleosome assembly on DNA measured in real time by single-molecule magnetic tweezers. *PLoS One*. 7:e46306. https://doi.org/10.1371/journal.pone.0046306

Zhao, H., R. Ghirlando, G. Piszczek, U. Curth, C.A. Brautigam, and P. Schuck. 2013. Recorded scan times can limit the accuracy of sedimentation coefficients in analytical ultracentrifugation. *Anal. Biochem.* 437:104–108. https://doi.org/10.1016/j.ab.2013.02.011

Zhao, H., G. Piszczek, and P. Schuck. 2015. SEDPHAT--a platform for global ITC analysis and global multi-method analysis of molecular interactions. *Methods*. 76:137–148. https://doi.org/10.1016/j.ymeth.2014.11.012

Zlatanova, J., C. Seebart, and M. Tomschik. 2007. Nap1: Taking a closer look at a juggler protein of extraordinary skills. *FASEB J.* 21:1294–1310. https://doi.org/10.1096/fj.06-7199rev

JCB

Supplemental material

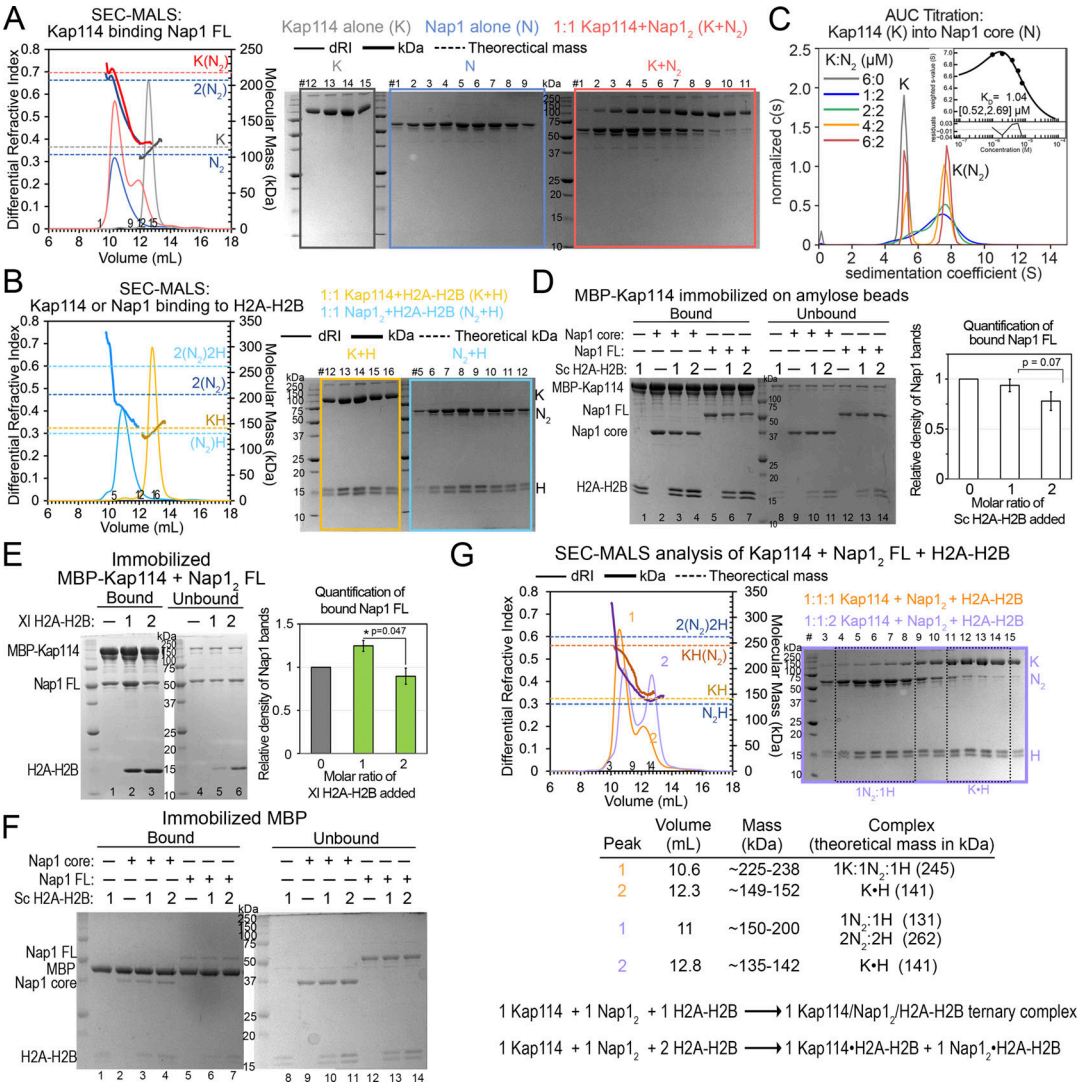

Figure S1. **Biochemical analysis of interactions between Kap114, Nap1, and H2A-H2B. (A)** SEC-MALS analysis of Nap1 FL (N; blue), Kap114 (K; gray), and a 1:1 mixture of both (red). Left panel: The differential refractive index (dRI) traces are plotted as thin lines (left y-axis) and the molecular mass (kDa) traces as thick lines (right y-axis). The theoretical masses of the indicated proteins are marked with dashed lines. Right panel, Coomassie-stained SDS-PAGE of peak fractions. Results: As previously reported, N alone formed tetramers with the apparent molecular mass of ~200 kDa (elution volume ~10.3 ml). K alone eluted at ~12.5 ml with the expected apparent molecular mass ~110 kDa. A 1:1 molar mixture of K and N_2 formed a peak of ~220 kDa that matches a K•N_2 complex. The increase in DRI signal of the K+N_2 compared to the N traces is consistent with incorporation of one K molecule. **(B)** SEC-MALS experiment for K (yellow) or N (cyan) binding to H2A-H2B (H) at the indicated molar ratios, plotted as in A. Results: K+H eluted with the expected molecular mass (elution volume ~13 ml), whereas the N_2+H mixture eluted at volumes that span molecular masses of 150–200 kDa, possibly due to a mixture of N_2•H, N_2•H_2 and 2(N_2•H) complexes. **(C)** AUC titration and binding isotherm (inset) of Kap114 (K; 5.2 S) into the Nap1 core dimer (N_2) at the concentrations indicated. Molecular weight estimate, using the c(s) distribution of the most saturated 6:2 M ratio sample of the 7.9 S complex was 178 kDa, consistent with a K•N_2 complex (theoretical molecular weight, 186 kDa). The isotherm was generated using a one-site binding model and fitting residuals are plotted below. The dissociation constant or K_D is shown with the values in brackets representing a 95% confidence interval. **(D)** The full gel of one of the two binding assays shown in Fig. 1 B: 1 μM immobilized MBP-Kap114 and Nap1_2 core or FL ± 1 or 2 μM *Sc* H2A-H2B. Bound and unbound proteins after extensive washing were visualized by Coomassie-stained SDS-PAGE. Quantification of the average relative intensities of triplicate experiments of the bound FL Nap1, when normalized to the sample without H2A-H2B, is plotted with error bars that indicate standard deviation (SD). Unpaired, two-sided Student's *t* test was performed. Data distribution was assumed to be normal but it was not formally tested. **(E)** Pull-down binding assay as in D, but with *Xl* H2A-H2B. Unlike *Sc* H2A-H2B, *X. laevis* (*Xl*) H2A-H2B increased *Sc* Nap1 association with Kap114, suggesting that different H2A-H2B homologs bind *Sc* Nap1 and Kap114 differently. Student t-test shows significant difference between 1 and 2 μM H2A-H2B samples, where less Nap1 was pulled down in the presence of excess H2A-H2B, suggesting destabilization of the ternary Kap114/Nap1_2/H2A-H2B complex. **(F)** Control pull-down experiment of 1 μM MBP (immobilized) and equimolar Nap1_2 ± H2A-H2B (1 or 2 M ratio). Background binding of Nap1 to the immobilized MBP was minimal. **(G)** SEC-MALS analysis of 1:1:1 (orange) or 1:1:2 (lilac) molar ratio K, N, and H mixtures, plotted as in A. Tabulated SEC-MALS results shown below. At 1:1:1 M ratio, most of the proteins assemble into a 1 Kap114/1 Nap1_2/1 H2A-H2B complex. There is a minor population of Kap114•H2A-H2B in peak 2, and thus there must be some excess Nap1_2 tetramers (~200 kDa) in peak 1. When H2A-H2B is in excess; only Kap114•H2A-H2B, Nap1_2/H2A-H2B complexes formed, as the peak centers match the two traces in B. In summary, both pull-down assays and SEC-MALS analysis support that excess H2A-H2B destabilizes a 1:1:1 Kap114/Nap1_2/H2A-H2B ternary complex, dissociating it into binary Kap114•H2A-H2B and Nap12•H2A-H2B complexes. Ternary Kap114/Nap1_2/H2A-H2B interactions, such as in the cytoplasm, maybe most stable when all H2A-H2B heterodimers are adequately chaperoned. Source data are available for this figure: SourceData FS1.

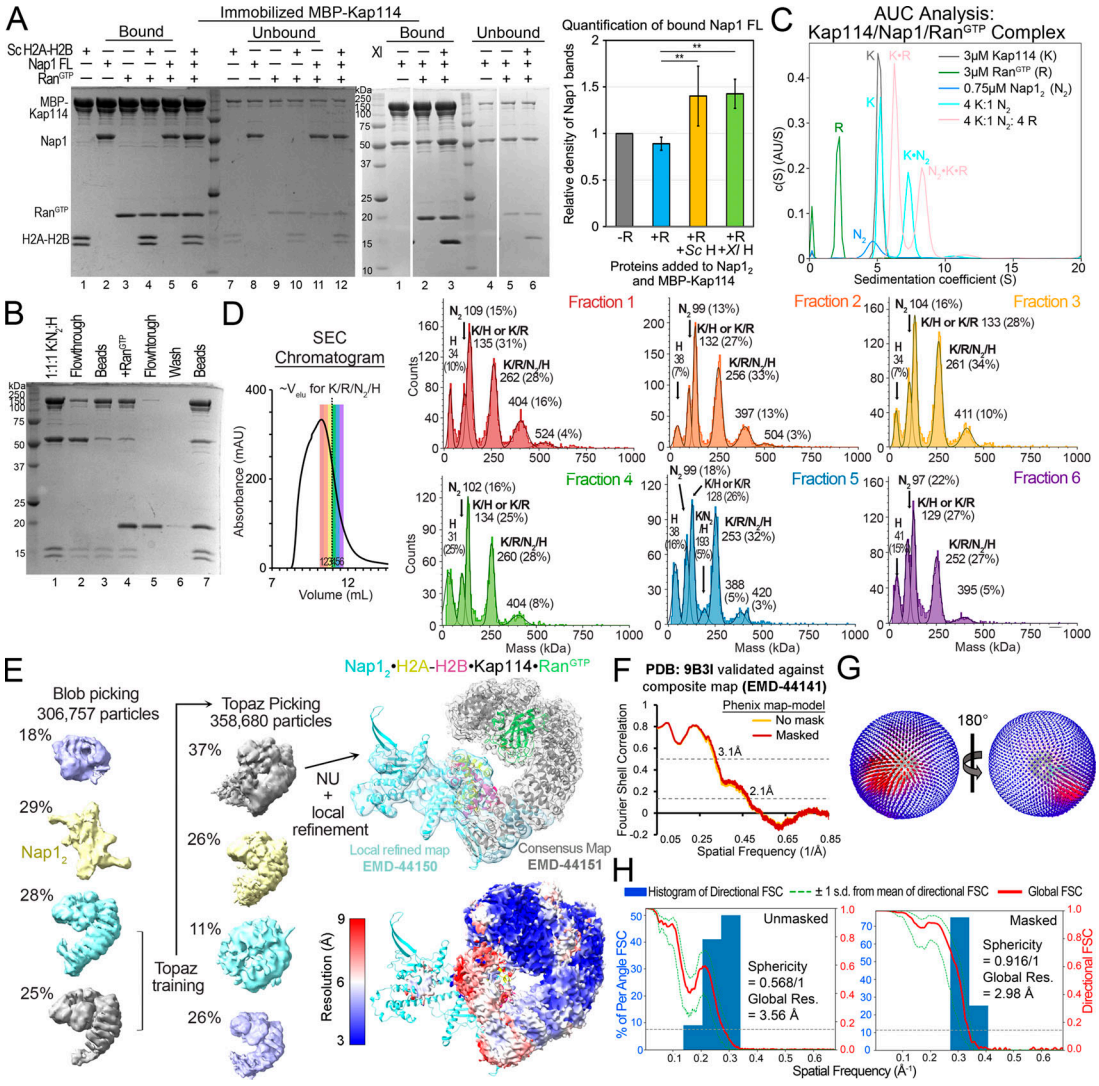

Figure S2. **Ran^{GTP} interaction with Kap114, Nap1$_2$, and H2A-H2B mixtures. (A)** The full gel of one of the two binding assays shown in Fig. 1 B, which is also similar to assays in Fig. S1, D and E. MBP-Kap114 (1 μM) was immobilized with equimolar Nap1$_2$ FL ± *Sc* or *Xl* H2A-H2B ± Ran^{GTP}. Quantification of the Kap114-bound Nap1 band intensities from triplicate experiments is shown on the right. ** indicate P value <0.01. Student's *t* test was performed two-tailed and unpaired. Data distribution was assumed to be normal but it was not formally tested. MBP-Kap114 pulled down more Nap1 when both H2A-H2B and Ran^{GTP} are present. This result is consistent with SEC-MALS data showing a smaller shoulder at the ~12.2 ml peak of the Nap1$_2$•H2A-H2B•Kap114•Ran^{GTP} trace (green; likely due to Kap114•H2A-H2B) than in the Nap1$_2$•H2A-H2B•Kap114 trace (orange) in Fig. 1 C. **(B)** The same pull-down assay as in A, except 3 μM Ran^{GTP} was added after pre-assembly of the MBP-Kap114/Nap1$_2$/H2A-H2B (K:N$_2$:H) complex and immobilization on beads. Individual steps of the binding assay are visualized by SDS-PAGE. The quaternary Kap114/Nap1$_2$/H2A-H2B/Ran^{GTP} complex formed regardless of the order of protein addition, and no Nap1 or H2A-H2B was dissociated by Ran^{GTP}. **(C)** AUC analysis of Kap114-Nap1 interaction in the presence of Ran^{GTP}. Plots of the c(s) distributions of unliganded proteins, Kap114 (K, 5.2 S), Nap1$_2$ core (N$_2$, 4.9 S) and Ran^{GTP} (R, 2.1 S), and mixtures of the proteins with indicated molar ratios. The species corresponding to the individual peaks are labeled. Ran^{GTP} binding increased sedimentation coefficient similarly for unliganded Kap114 (K, 5.2 → K•R, 6.3S) and for Kap114•Nap1$_2$ (K•N$_2$, 7.3 → N$_2$•K•R, 8.3S). The Kap114•Ran^{GTP} and Nap1$_2$•Kap114•Ran^{GTP} complexes had estimated molecular weights of 138 and 206 kDa, respectively, consistent with equimolar complexes. **(D)** Left: SEC chromatogram of the Kap114/Nap1$_2$/H2A-H2B/Ran^{GTP} sample. Kap114, Nap1$_2$, H2A-H2B, and Ran^{GTP} were mixed in equimolar ratio and dialyzed overnight before mild crosslinking. Fractions 1–6 of the SEC chromatogram are colored red to purple, and the typical elution volume of a non-crosslinked complex that contains all four proteins is marked with a dotted line. Right: Mass photometry traces of each of the six SEC fractions, with mean masses (kDa) and relative populations (%) indicated above the fitted gaussian peaks, along with the likely protein or complex that correspond to the approximate masses. Fraction 3, most enriched with the complex containing Kap114, Nap1$_2$, H2A-H2B and Ran^{GTP}, was used for cryo-EM grid preparation. The largest (~380–410 kDa) species in each of the six SEC fractions may contain crosslinked complexes of K/R/N$_2$/H with K•R; such a large assembly was not observed in AUC or SEC-MALS analyses where the proteins were not crosslinked. **(E)** Particle distribution of cryo-EM data obtained for the quaternary Kap114/Ran^{GTP}/Nap1$_2$/H2A-H2B complex. Blob picking was used first and then the particles containing Kap114 and Ran^{GTP} were used for Topaz training. Topaz-picked particles were cleaned up and submitted for 3D reconstruction to obtain four maps. The population with density for H2A-H2B and Nap1$_2$ (albeit poor density) was used for non-uniform (NU; gray map; EMD-44151) and local refinement (cyan map; EMD-44150) to obtain the final maps. The maps were overlayed onto the final Nap1$_2$•H2A-H2B•Kap114•Ran^{GTP} structure (9B3I; in cyan•yellow-red•gray•green). Below is the consensus map colored by local resolution. **(F)** Phenix map-to-model FSC curves for the composite map (EMD-44141). **(G)** 3D angular distribution of the particles used for reconstruction. Left orientation is the same as in E. **(H)** Directional FSCs unmasked and masked by cryoSPARC refine mask, for the consensus map. Source data are available for this figure: SourceData FS2.

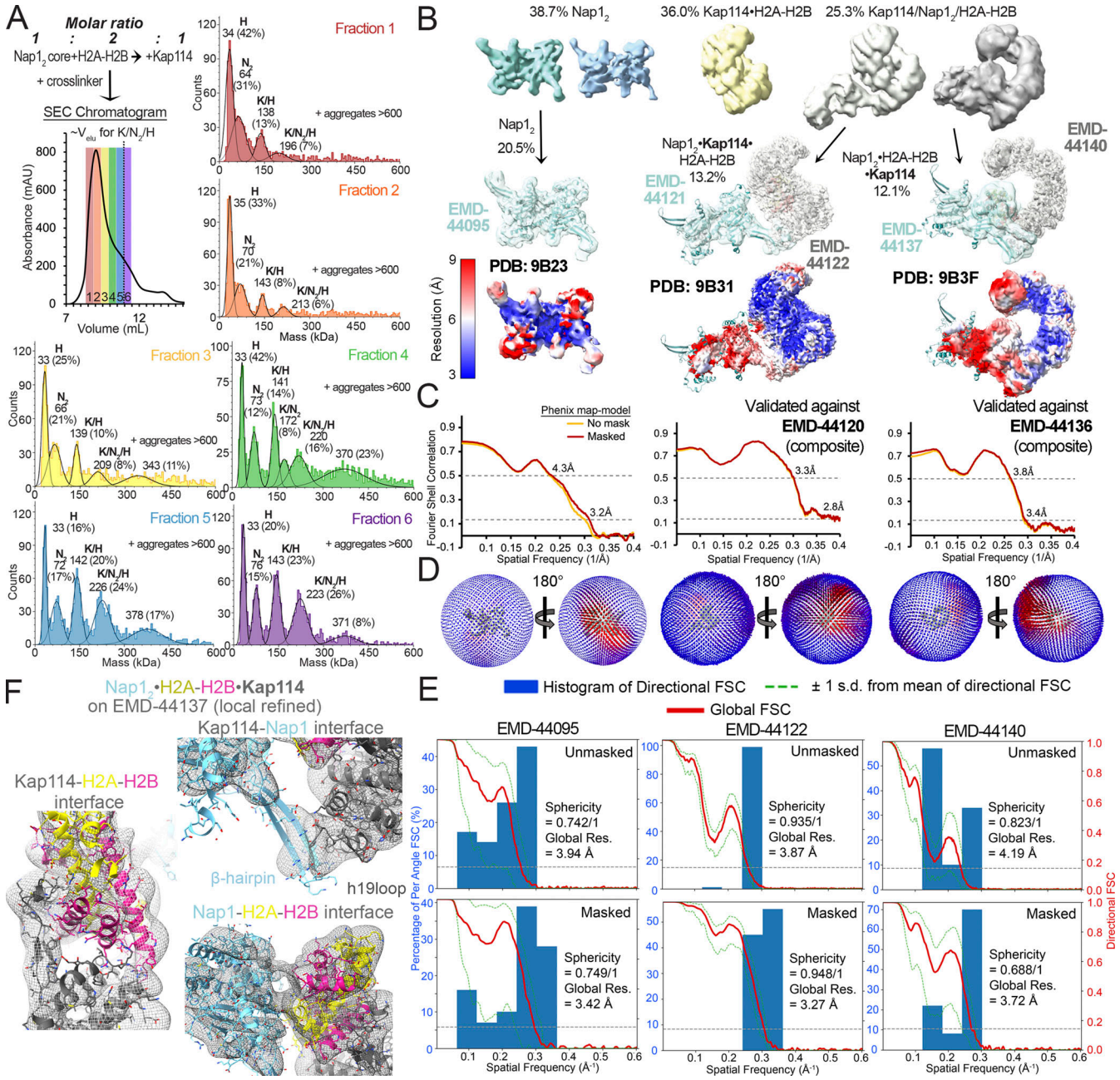

Figure S3. **Cryo-EM analysis of the Kap114/Nap1$_2$/H2A-H2B ternary complexes. (A)** Top left: Schematic of how the cryoEM sample was assembled with its SEC chromatogram below, with fractions 1–6 colored red to purple. The typical elution volume of an uncrosslinked complex of Kap114, Nap1$_2$, and H2A-H2B is ~11 ml (dotted line). Each fraction was analyzed by mass photometry, and the data are plotted as in Fig. S2 D. Protein aggregates beyond 600 kDa were not displayed. Proteins in the ~340–380 kDa peak may be crosslinked complexes of K/N$_2$/H with K/H; such a large complex was not observed in AUC or SEC-MALS studies. Fraction 6, most enriched with the 1:1:1 Kap114:Nap1$_2$:H2A-H2B complex and has the least large aggregates, was used for cryo-EM grid preparation. **(B)** Distribution of the ~1 million particles produced by the cryo-EM data: 38.7% are Nap1$_2$, 36.0% Kap114•H2A-H2B, and 25.3% ternary complex of Kap114/Nap1$_2$/H2A-H2B (see more statistics in Table S1). The small population of ternary complex is likely due to destabilization of the assembly by excess H2A-H2B as shown in Fig. S1. Ternary complex particles were classified into two evenly divided classes that produced two high-resolution maps and structures. Left to right: Final consensus maps for Nap1$_2$ (EMD-44095; cyan) overlayed with the final model (9B23; cyan), consensus (EMD-44122; gray) and local refined (EMD-44121; cyan) maps for Nap1$_2$•Kap114•H2A-H2B overlayed with the final model (9B31; cyan•gray•yellow-red), and consensus (EMD-44140; gray) and local refined (EMD-44137; cyan) maps for Nap1$_2$•H2A-H2B•Kap114 overlayed with the final model (9B3F; cyan•yellow-red•gray). Consensus maps are also shown below colored by local resolution. Nap1$_2$•Kap114•H2A-H2B resembles the Kap114•H2A-H2B structure (8F0X), with Nap1$_2$ contacting Kap114 h19loop via the β-hairpin. This structure may represent a ternary complex that is falling apart or it may be one configuration of a dynamic ternary complex ensemble. **(C)** Left to right: Phenix map-to-model FSC curves for the consensus map for Nap1$_2$, or the composite maps for Nap1$_2$•Kap114•H2A-H2B (EMD-44120) and Nap1$_2$•H2A-H2B•Kap114 (EMD-44136). **(D)** 3D angular distribution of the particles that were used for reconstructions of the consensus maps above. The left orientation is same as in B. **(E)** Directional FSCs unmasked and masked by cryoSPARC refine mask of the consensus maps above. **(F)** The Nap1$_2$•H2A-H2B•Kap114 structure overlayed onto the local refined map (gray mesh), zoomed into the Kap114-H2A-H2B, Kap114-Nap1$_2$ and Nap1$_2$-H2A-H2B interfaces.

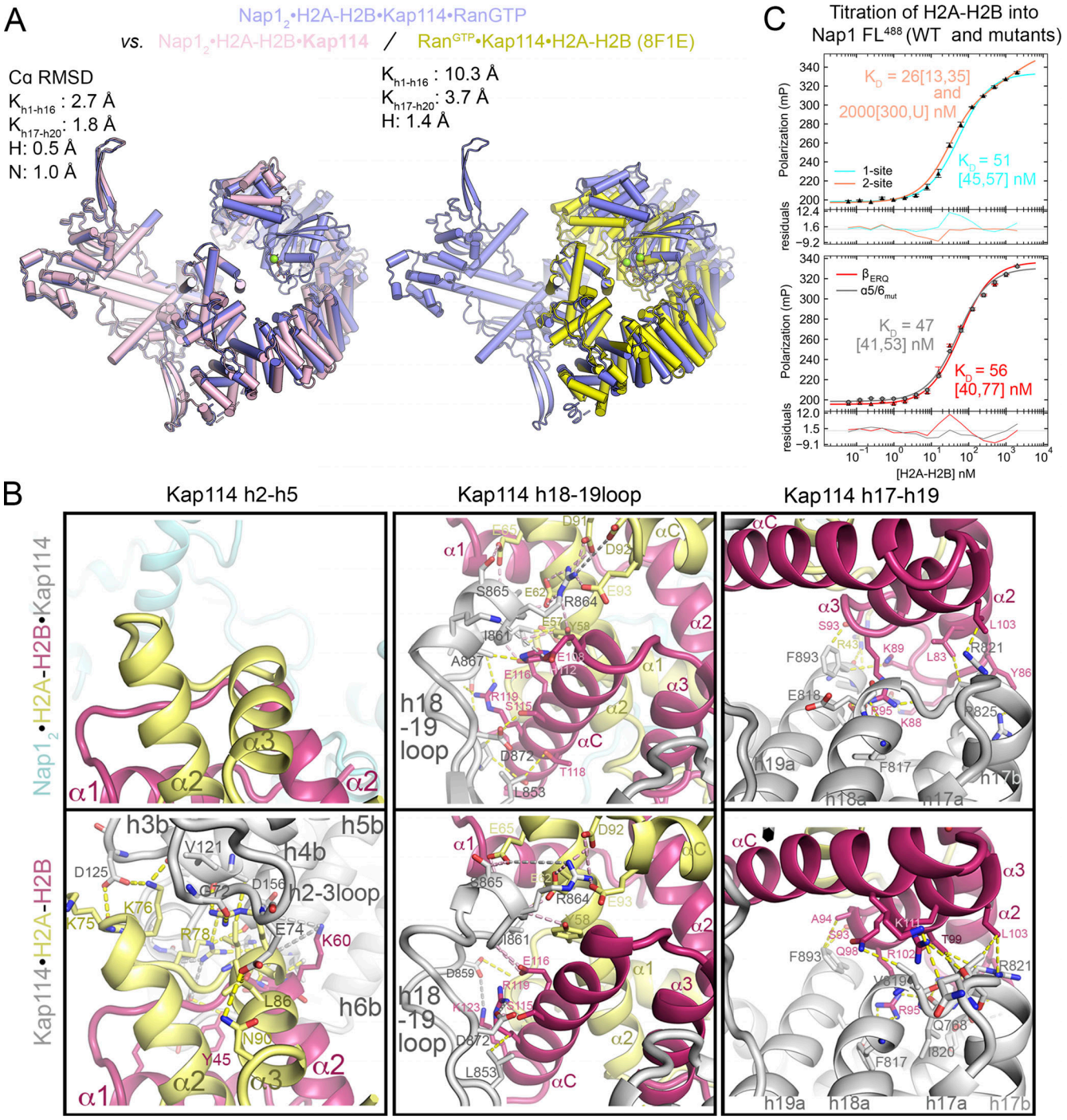

Figure S4. **Structural comparisons of Nap1$_2$•H2A-H2B•Kap114•Ran^{GTP} with other structures. (A)** The H2A-H2B heterodimers of Nap1$_2$•H2A-H2B•Kap114•Ran^{GTP} (purple), Nap1$_2$•H2A-H2B•Kap114 (pink; left) and Ran^{GTP}•Kap114•H2A-H2B (yellow; right, PDB: 8F1E) were aligned. The Cα r.m.s.d. values of different molecules, calculated in PyMOL without realignment, are reported. **(B)** Left to right: Interactions of H2A-H2B with HEAT repeats 2–5 of Kap114 or lack thereof, and the persistent interactions with h18-19loop of Kap114 and h17-h19 in Nap1$_2$•H2A-H2B•Kap114 and Kap114•H2A-H2B (PDB: 8F0X). **(C)** Nap1 mutations at its interfaces with Kap114 or H2A-H2B in Nap1$_2$•H2A-H2B•Kap114 do not affect H2A-H2B binding as seen in fluorescence polarization assay using 10 nM Nap1$_2$ FL labeled with XFD488 (Nap1 FL^{488}). Data points are averages ± SD. of triplicate measurement. Top: WT Nap1 tiration. The lines show data fitted with one- or two-site binding and residuals are plotted below. Dissociation constants are recorded with the 95% confidence interval obtained by error-surface projection method in brackets. The data is better fitted with two-site binding, which is consistent with previous works by Ohtomo et al. that reported human Nap1$_2$ binding two copies of H2A-H2B, one bound to the C-terminal acidic tails and one to the core. Bottom: Nap1 mutants β_{ERQ} and α5/6$_{mut}$. One-site binding model was used for fitting as data could not be fitted confidently with two-site binding. All Nap1 mutants bound H2A-H2B with high affinity in the low nM range.

Provided online are Table S1 and Table S2. Table S1 shows cryoEM data collection, refinement and validation statistics for the Nap1 core and $Nap1_2$•Kap114•H2A-H2B structure. Table S2 lists primers used in this study.